High Potency Drug Screening in Neuroendocrine Prostate Cancer

A Thesis Submitted to the College of
Graduate and Postdoctoral Studies
In Partial Fulfillment of the Requirements
For the Degree of Masters of Science
In the Department of Pharmacology
University of Saskatchewan
Saskatoon

By

Raymond Khan

PERMISSION TO USE

In presenting this thesis/dissertation in partial fulfillment of the requirements for a Postgraduate degree from the University of Saskatchewan, I agree that the Libraries of this University may make it freely available for inspection. I further agree that permission for copying of this thesis/dissertation in any manner, in whole or in part, for scholarly purposes may be granted by the professor or professors who supervised my thesis/dissertation work or, in their absence, by the Head of the Department or the Dean of the College in which my thesis work was done. It is understood that any copying or publication or use of this thesis/dissertation or parts thereof for financial gain shall not be allowed without my written permission. It is also understood that due recognition shall be given to me and to the University of Saskatchewan in any scholarly use which may be made of any material in my thesis/dissertation.

DISCLAIMER

The BioMek, Molecular Devices, V&P Scientific and Targetmol were exclusively created to meet the thesis and/or exhibition requirements for the degree of Masters of Science at the University of Saskatchewan. Reference in this thesis/dissertation to any specific commercial products, process, or service by trade name, trademark, manufacturer, or otherwise, does not constitute or imply its endorsement, recommendation, or favoring by the University of Saskatchewan. The views and opinions of the author expressed herein do not state or reflect those of the University of Saskatchewan, and shall not be used for advertising or product endorsement purposes.

Requests for permission to copy or to make other uses of materials in this thesis/dissertation in whole or part should be addressed to:

Head of the Department of Pharmacology
107 Wiggins Road
University of Saskatchewan
Saskatoon, Saskatchewan S7N 5E5
Canada

OR

Dean
College of Graduate and Postdoctoral Studies
University of Saskatchewan
116 Thorvaldson Building, 110 Science Place
Saskatoon, Saskatchewan S7N 5C9
Canada

Abstract

Neuroendocrine Prostate Cancer (NEPC) is an aggressive subtype of prostate cancer, affecting approximately 2% of all prostate cancer patients. While NEPC is a rare disease, it has no known treatment and often leads to death within a year of diagnosis. As result of low incidence rates, these rare conditions typically do not get the same pharmaceutical interest, as discovery research rarely recovers the cost for development and clinical trials. Drug repurposing is a viable option for rare conditions and the use of high-throughput screens can lead to drug repurposing discovery. Chemotherapy has moved to personalize therapy, focusing on molecular alterations for specific tumors. NEPC cell lines (specifically, LnCAP and 22rv1) have been shown to overexpress n-MYC (MYCN), which is a proto-oncogene not typically expressed in adult tissue. This transcription factor is typically present in developing tissue that results in neural tissue. The LnCAP cell lines (LnCAP-P and LnCAP-n-MYC) have been shown to be a *in vitro* NEPC model, and along with Benign Prostate Hyperplasia tissue (BPH-1) as a control, these cell lines were screened using the Targetmol Drug library, which contained 1813 small molecules at concentrations of 100 nM, 500 nM and 1000 nM in 384-well optic plates using high-throughput microscope and RFP fluorescence in cell lines. Fludarabine and Fludarabine phosphate were identified as potential n-MYC selective hits and validation of Fludarabine phosphate using Alamar Blue viability reagent in 96-well plates were done using BPH-1, LnCAP, and 22rv1. Result confirmed Fludarabine phosphate selectively inhibited cell viability in n-MYC overexpressed cells in both LnCAP and 22rv1.

Acknowledgements

I would like to thank my supervisor, Dr. Franco Vizeacoumar, and the Saskatchewan Cancer Agency from the University of Saskatchewan for this tremendous opportunity. I would also like my Advisory Committee members; Dr. Andrew Freywald, Dr. Changiz Taghibiglou, and Dr. Venkat Gopalakrishnan for the guidance throughout my Master's. For those that helped with the project; Mr. Bjorn Haave, Mr. Deepanshu Sharma, and Dr. Kalpana Kalyanasundaram Bhanumathy thank you for all that you contributed to the project. But a special thanks to Dr. Nezeka Alli and Mr. Frederick Vizeacoumar; I cannot thank you enough for your advice, teaching, and contributions to this project.

Dedication

This thesis is dedicated to my wife and best friend, as well as to my parents. You have always been a constant source of support and encouragement during the aspiration of my dreams, despite the many obstacles. I am truly grateful for having you in my life.

Title of Contents

List of Tables

List of Figures

1. Statement of Objectives

The purpose of the research project was to investigate the scientific usefulness of high-throughput screening in repurposing a small molecule for the treatment of Neuroendocrine Prostate Cancer (NEPC) that exhibits n-MYC overexpression. The high-throughput screen took advantage of imaging rather than endpoint screens, as it allowed for detection of inhibition onset as well as the duration of inhibitory effect. The screen was also with nanomolar concentrations as one of the primary challenges with high-throughput screens is the risk of toxicity. Successful molecular concentrations *in vitro* typically exceed clinical therapeutic range. Therefore, *in vitro* screens that identify small molecule targets in the nanomole range have a higher likelihood of success transitioning to *in vivo* or clinical studies.

NEPC is a rare oncology condition that develops in response to androgen deprivation therapy for prostate adenocarcinoma. Rare conditions, such as NEPC, often lack motivation for pharmaceutical discovery research since the returns on such research rarely cover costs associated with the investment. Drug repurposing is a viable option for rare conditions, as there are no capital costs as they were involved in original drug discovery. Repurposing also can provide insight into the underlying mechanism for tumor growth, aggressiveness, and therapeutic resistance.

NEPC currently has no known therapy, while chemotherapy agents are still being used in the hopes to prolong the patient's life. But cancer therapy has transitioned from a "shotgun" approach to a targeted approach based on molecular alterations specific to individual cancer types. This approach is beneficial to the patient, not only by reducing adverse effects, but also enables treatment of metastatic disease that exhibits the same molecular alteration. While radiation and surgery is still a viable option for localized disease, they are not indicated for metastatic disease. One of the hallmarks of NEPC is the overexpression n-MYC (MYCN), which is a transcription factor from proven oncogene family of MYC and is associated with a variety of cancer types, specifically associated with the neural system. A key characteristic of n-MYC is that is not typically expressed in normal adult tissue, making it a potential ideal molecular target

for personalized chemotherapy. Another key characteristic of NEPC is that it typically presents with visceral and distant metastasis and therefore, a personalized chemotherapy that targets n-MYC can potentially target metastatic tumors without the need for multiple surgeries.

1.1 Thesis Statement

High-throughput drug screen has led to the discovery of Fludarabine Phosphate as a potential targeted chemotherapy agent for Neuroendocrine Prostate Cancer that overexpresses n-MYC.

2. Critical Review of Relevant Literature

Neuroendocrine Prostate Cancer (NEPC) is a subtype of prostate cancer and is one of the most aggressive forms of cancer. Currently, there is no mainstream therapy for patients with this terminal disease and life expectancy once diagnosed is less than 12 months.

> "If you do not know where you come from, then you don't know where you are, and if you don't know where you are, then you don't know where you're going. And if you don't know where you're going, you're probably going wrong."
>
> ~ Terry Pratchett

Invariably, NEPC originates from prostate adenocarcinoma, which is the most common cancer in men and the leading cause of cancer-related mortality in men. The most common cause of death from prostate adenocarcinoma is due to metastatic progression.[1] As such, understanding prostate adenocarcinoma as a whole is important to the understanding of NEPC and the future direction for treatment.

2.1 Prostate Cancer

Cancer itself is the leading cause of mortality in Canada. There are two fundamental forms of prostate cancer; adenocarcinoma and squamous cell carcinoma. Adenocarcinoma accounts 95% of cases, which develops from the secretory cells of the prostate. Prostate adenocarcinoma is an androgen-dependent disease, which results in the mainstay therapy of androgen deprivation.[2, 3]

2.1.1 Epidemiology of Prostate Adenocarcinoma

Prostate Adenocarcinoma is the leading cause of mortality in men worldwide, with the most common cause of death due to metastatic progression.[1] Figure 2.1 was derived from Cancer Canada, which summarizes 2012 Canadian mortality etiology's and 2017 Canadian male cancer incidence.[4] In 2012, cancer accounted for over 30% of Canadian deaths, surpassing heart and cerebrovascular disease combined. Of the various types of cancer, prostate cancer accounted for 1 in 5 newly diagnosed cases of cancer in men. In 2017, prostate cancer accounted 20.7% of all new cancer diagnosis, with over 100,000 new cases.[4] The increase in incidence since the nineties can be attributed to the increased use of prostate-specific antigen (PSA) in screening, which has shown men of African descent representing the highest observed incidence rates. But the 2013 Cochrane meta-analysis show no reduction in prostate related mortality from the use of PSA screening.[5, 6] However, there has been significant evidence for over-diagnosis and over-treatment as result of PSA screening since elevated PSA can detect small, slow-growing tumors that are non-life-threatening.[7-10]

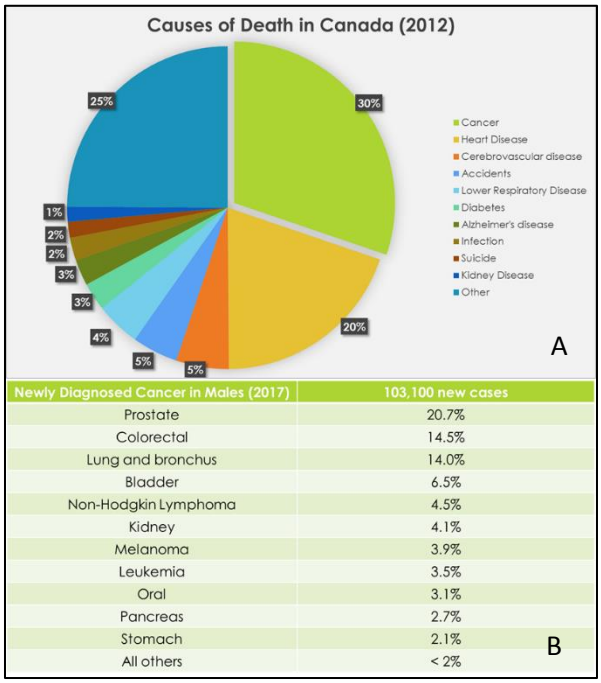

Newly Diagnosed Cancer in Males (2017)	103,100 new cases
Prostate	20.7%
Colorectal	14.5%
Lung and bronchus	14.0%
Bladder	6.5%
Non-Hodgkin Lymphoma	4.5%
Kidney	4.1%
Melanoma	3.9%
Leukemia	3.5%
Oral	3.1%
Pancreas	2.7%
Stomach	2.1%
All others	< 2%

B

Figure 2.1. Cancer Canada Statistics. A) 2012 mortality for Canadian etiology's. B) 2017 male cancer incidence rates.

Currently, prostate cancer accounts for 10% of all cancer diagnosis and has a lifetime risk of 12%, which approximates about 4.5% of all cancer-related deaths. There are approximately over 3 million men living with prostate cancer in the United States alone, as the relative 5-year survival rate for localized prostate cancer is 98.6%. Approximately, 98% to 96% of patients are alive after 10 to 15 years, respectively. But the survival rates drop dramatically to 29% 5-year survival rate if metastasis is present.[11]

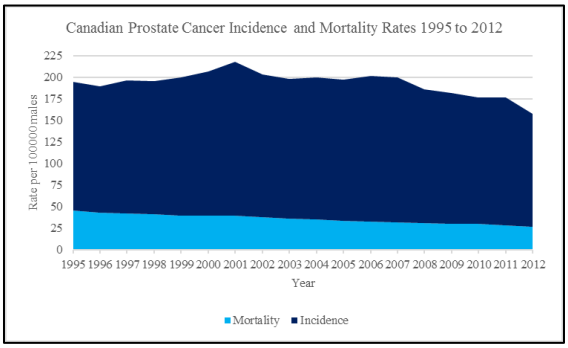

Figure 2.2 Cancer Canada Statistics. Canadian prostate cancer incidence rates vs. mortality rates from 1995 to 2012.

Figure 2.2 was derived from Cancer Canada and illustrates the fluctuation in prostate cancer incidence while showing a steady decline in mortality from 1995 to 2012. Looking at the Canadian statistics from 1995 to 2012, the incidence rates began to rise in the mid-nineties, while the mortality rates have shown a steady decline.[4] The study performed by Dr. Brawley showed a similar trend in incidence rates in the United States, but also showed higher rates in African American males compared to Caucasians males, in both incidences and mortality rate. Figure 2.3 was derived from the National Cancer Institute Surveilance Epidemiology and End Results, which illustrates the higher prostate incidence and mortality rates in African American males compared to all other races, as well higher risk in African American males as they age.[12] The study also showed that incidence and mortality rates

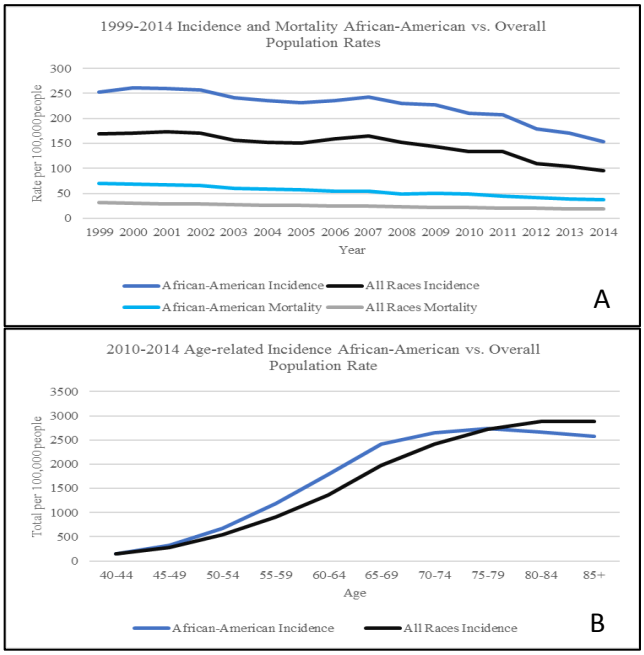

Figure 2.3 National Cancer Institute Statistics. A) Comparison between African American vs. All races from 1999-2014. Prostate cancer incidence and mortality rates were compared B) Comparison between African American prostate vs. All races from 2010-2014. Incidence rates were compared with regards to age.

increased with age, peaking at 70-74 years for African Americans and 85+ years for all other races.[12, 13]

Risk factors for prostate adenocarcinoma include a family history of prostate cancer, African-decent population, and age. Men are 2-3 times more likely to be diagnosed when a first-degree relative has been diagnosed with prostate cancer. With regards to age, men below the age of 60 have less than a 40% risk, while there is a 25-65% risk after the age of 60.[14, 15] Therefore, there is a higher incidence rate in African-American compared to the rest of the population, as well as the increased risk associated with age.[12, 13]

2.1.2 Pathophysiology of Prostate Adenocarcinoma

Clinically, prostate adenocarcinoma presents with urological obstructive symptoms. Patients often complain of difficulty with urination, such as issues starting urination, weak or interrupted flow or difficulty emptying bladder. Patients may also have increased frequency of urination, especially at night, as well as pain during urination that may or may not have blood in the urine. Pain may also be present in the lower back, hips or pelvis, and may also occur during intercourse and ejaculation.[10, 15]

Prostate adenocarcinoma is graded based on the methodology developed by Dr. Donald Gleason in the 1960's.[16] This grading system has evolved over the years and in 2014, the International Society of Urologic Pathology instituted the current guidelines used today.[17] Changes to the Gleason scoring system has improved the report reproducibility and the accuracy of the risk stratification. Currently, two scores are given for the pathology; the first score is the most predominant pattern found in the biopsy, while the second score is the second predominant pattern.[16]

Table 2.1 Summary of the 2014 Gleason Grade Assignment[16]

Gleason Group	Gleason Score	Description
Non-Assigned	Scores 2-5	Biopsies are well differentiated (glands are small, uniform, but portions of stroma can be enlarged between glands)
Group 1	Combined Scores 6	Biopsies are moderately differentiated glands (stroma is enlarged between glands)
Group 2	Combined Scores 7 (3+4)	Biopsies transition from moderately to poorly differentiated (infiltration of cells from glands and irregular masses with few glands)
Group 3	Combined Scores 7 (4+3)	Biopsies transition from moderately to poorly differentiated (infiltration of cells from glands and irregular masses with few glands)
Group 4	Combined Scores 8	Biopsies transition from poorly differentiated to anaplastic (entire biopsy shows irregular masses of neoplasia
Group 5	Combined Scores ≥ 9	Biopsies are anaplastic (lack of glands)

A common molecular characterization of prostate adenocarcinoma is the presence of ETS-related gene (ERG) fusion, which was characterized via immunohistochemistry (IHC) and fluorescence in situ hybridization (FISH).[18] ERG gene fusion is limited to only prostate adenocarcinoma and is driven by androgen receptor signaling.[18, 19] ERG gene is an oncogene and codes for ERG, which is a transcriptional regulatory protein. ERG belongs to the erythroblast transformation-specific (ETS) family of transcription factors, which is regulates several functions, including cell proliferation and apoptosis.[1, 18] ERG gene fusion commonly rearranges with the TMPRSS2 gene, which is a prostate-specific molecular alternation, as its seen in over 50% of cases of prostate adenocarcinoma.[1]

Prostate Adenocarcinoma is primarily an androgen-dependent disease, therefore it is logical that the standard treatment involves androgen deprivation by either surgical or medical castration.[20] Hormonal therapy for metastatic prostate cancer was first introduced in the 1960's by Huggins et al.[21] The majority of androgen synthesis occurs in the testes, with a small fraction originating from the adrenal glands. The growth of prostate cancer cells is promoted by androgen binding to androgen receptors, which can also be stimulated from dehydroepiandrosterone (DHEA) and androstenedione, which are products of the adrenal gland and can be converted to androgens in prostate cancer cells.[22]

The testes produce sex steroids that are required gametogenesis, secondary sexual characteristics, and reproduction, while the zona reticularis of the adrenal gland produces androgens; specifically dehydroepiandrosterone (DHEA), DHEA-sulphate (DHEA-S) and androstenedione.[23] But neither DHEA or DHEA-S can activate androgen receptors directly. They are converted to testosterone and dihydrotestosterone in the peripheral tissue.[24] Figure 2.4 illustrates the overall pathway for testicular testosterone production, which begins with the secretion of gonadotropin-releasing hormone (GnRH) from the hypothalamus, which stimulates the anterior pituitary gland to release follicle stimulating hormone (FSH) and luteinizing hormone (LH). FSH acts on Sertoli Cells in the testes, which are responsible for spermatogenesis, while LH acts on Leydig cells, which are involved in testosterone production.[25] High-density lipoproteins (HDL) bind to the scavenger receptor class B type 1 (SR-B1) found on Leydig cells in response to LH. As result, cholesterol is converted to pregnenolone via CYP11A (P450scc) within the mitochondria, which is regulated by steroidogenic acute regulatory proteins (StAR). [26] Pregnenolone then enters the endoplasmic reticulum, which is then converted to testosterone via several enzymatic reactions.[25] Figure 2.5 illustrates the enzymatic pathway found in Leydig cells, which begins with conversion of cholesterol to pregnenolone via P450scc in the mitochondria. Pregnenolone enters the endoplasmic reticulum, where it is converted to progesterone via 3β hydroxysteroid dehydrogenase and 17α- hydroxypregnenolone via P450c17 17α-hydroxylase, which also converts progesterone to 17α-hydroxyprogesterone. 17α-hydroxypregnenolone can be converted to 17α-hydroxyprogesterone, or it can be converted to dehydroepiandrosterone via P450c17 17,20-lyase, which also converts 17α-hydroxyprogesterone to androstenedione. Dehydroepiandrosterone can be converted directly to androstenedione, or it can be converted to androstenediol via 3β hydroxysteroid dehydrogenase. Testosterone is made via 17β hydroxysteroid dehydrogenase enzymatic activity on androstenediol or androstenedione.[25, 26]

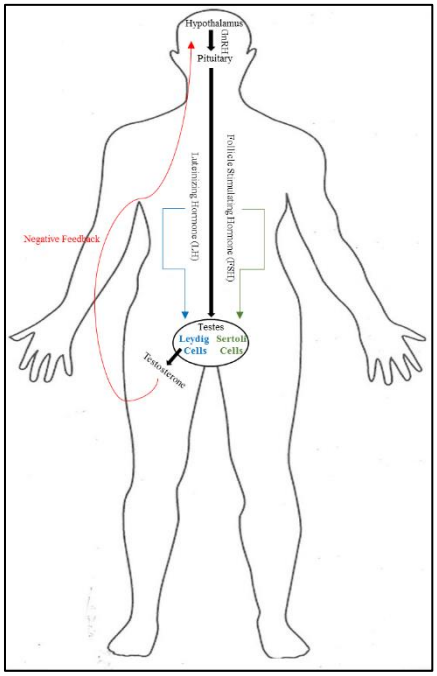

Figure 2.4. Testicular testosterone production. Leydig cells produce testosterone after stimulation from the anterior pituitary gland.

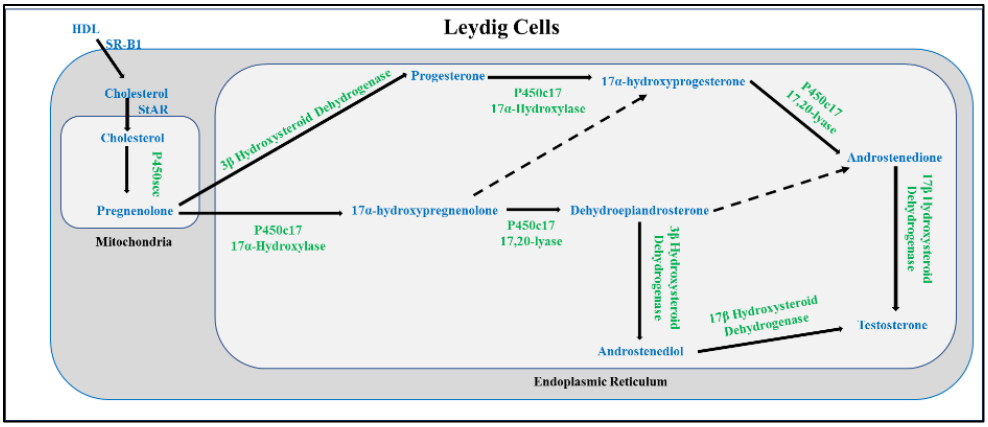

Figure 2.5. Testosterone pathway in Leydig cells of the testis. Cholesterol is converted to testosterone via several enzymatic steps, which also form testosterone intermediates.

Adrenal testosterone begins with stress causing the hypothalamus to release corticotropin-releasing hormone (CRH), which stimulates the anterior pituitary gland to release adrenocorticotropic hormone (ACTH) to act on the adrenal cortex. Cholesterol is converted to pregnenolone in the zona glomerulosa, which is converted to DHEA and androstenedione in the zona reticularis.[23] Both DHEA and androstenedione are then converted to testosterone within the Leydig cells of the testes. Chronic maintenance of this activity is mediated by ACTH, which can fluctuate androgen levels compared to androgens production due to LH.[24]

2.1.3 Management of Prostate Adenocarcinoma

The first-line treatment for advanced prostate adenocarcinoma is androgen deprivation via chemical castration with antiandrogen pharmaceuticals or by surgical castration by bilateral orchiectomy.[3] Huggins and colleagues first reported the clinical benefits of androgen blockage by surgical castration, but currently, castration is accomplished by pharmaceutical therapy.[21] Combined antiandrogen treatment is achieved by inhibiting androgen binding to androgen receptors or the decrease of androgen production either by suppressing formation of testosterone or inhibiting androgen synthesis, with the suppression of testosterone formation being more effective in prostate cancer.[27] Also, non-steroidal antiandrogens show a higher efficacy and affinity for androgen receptors and therefore have a strong suppressive effect.[20, 28]

There are 5 major classes of pharmaceutical agents used for androgen deprivation in prostate cancer; luteinizing hormone-releasing hormone agonist (LH-RH agonist), luteinizing hormone-releasing hormone antagonists (LH-RH antagonists), antiandrogens, CYP17 inhibitors, and estrogen.[29] LH-RH agonists, such as goserelin acetate, continuously stimulates pituitary receptors leading to receptor downregulation and disruption of hypothalamic-pituitary-testis axis. Goserelin acetate has similar effectiveness as bilateral orchiectomy and is cleared via hepatic and renal elimination.[29, 30] Clinically, LH-RH agonist causes a 'flare phenomenon' in the first 2 weeks, which results in a surge of testosterone from the initial increase of LH. As a result, symptoms can worsen, and clinicians typically add antiandrogens or estrogen to prevent flare.[29] LH-RH agonists leads to desensitization and suppression of gonadotropin release, and the most common and tested GnRH agonist used in prostate adenocarcinoma is Leuprolide. Besides testosterone synthesis suppression via decrease LH, there is also a reduction of FSH and consequently, decrease spermatogenesis. Other side-effects include hot flashes, sweats, testicular shrinkage and elevated blood sugars.[31]

LH-RH antagonists, such as degarelix, cause reversible suppression of gonadotropin by competing with binding sites. LH-RH antagonists cause direct inhibition, and therefore does not lead to 'flare phenomenon', as are also used along with prednisone to treat Castration-Resistant Prostate Cancer (CRPC).[29, 30] But typically, the androgen deprivation mode that is used for CRPC is antiandrogens. Antiandrogens are broken into two categories; steroidal and nonsteroidal. Steroidal androgen receptor antagonists, such as cyproterone acetate, have direct competitive inhibition as well as indirect testosterone synthesis inhibition via negative feedback on gonadotropin secretion.[32] Cyproterone acetate does not undergo first-pass metabolism, with 100% bioavailability, but currently used outside of the United States, as it is not currently FDA approved. Nonsteroidal androgen receptor antagonists, such as enzalutamide, competitively binds to androgen receptors causing inactivation of cellular receptor without any hormonal activity.[29] Patients are typically pretreated with nonsteroidal androgen receptor antagonists before LH-RH agonists to prevent testosterone flare. Use of non-steroidal androgen receptor antagonists is typically used in Castrate-Resistant Prostate cancer to treat metastasis. The use of steroidal androgen receptor is typically used clinically since they have poor bioavailability, potential liver toxicity and potential cross-reactions with other steroid receptors.[33]

The fourth class include CYP17 inhibitors, which competitively inhibit CYP17 and several other cytochrome P450 enzymes, and as a result, inhibits testosterone synthesis in adrenal and gonads. CYP17 inhibitors, such as ketoconazole, are used to treat CRPC and are typically given with hydrocortisone to reduce adverse effects.[29] Abiraterone acetate is a steroidal CYP17A1 inhibitor and is the most commonly used testosterone synthesis inhibitor in prostate cancer.[34] Estrogens are the final class of androgen deprivation drugs used for prostate cancer. Diethylstilbestrol (DES) is a semisynthetic estrogen that inhibits hypothalamic-pituitary-testis axis, and while DES was used in the 1940's to cause medical castration for prostate cancer patients, it is no longer used due to cardiovascular and thromboembolic events.[29]

With the rise in life expectancy for North Americans, prostate cancer is a major public issue with significant medical and financial repercussions.[35] Typically, once a patient has been placed on androgen deprivation therapy for prostate adenocarcinoma, they are continued on this treatment for the remainder of their life. In 1998, the Canadian healthcare system spent over $77 million on hospital expenses and approximately $26 million on pharmaceutical treatment associated with prostate cancer.[36] Typically, the majority of the costs occur within the first year after patients have been diagnosed with prostate cancer. After which, pharmaceutical treatment accounts for over 60% of the financial costs associated with the continuing-care of these patients.[35] Unfortunately, drug resistance to antiandrogen therapy is now becoming more prominent with the use of prolonged androgen deprivation. Once prostate adenocarcinoma becomes resistant to androgen deprivation, it is then considered CRPC.[37]

2.1.4 Castration-Resistant Prostate Adenocarcinoma (CRPC)

Prostate cancer is becoming the most frequent solid tumor in men due to early detection and increased life expectancy and as a result, is the leading cause of cancer-related death in males.[38, 39] While most patients respond to androgen deprivation, a growing number of patients are developing resistance to androgen deprivation, which leads to the development of Castration-Resistant Prostate Cancer (CRPC) in approximately 18% of cases.[40] In CRPC, cancer progresses despite androgen receptor inhibition and low levels of serum testosterone.[19] CRPC tumors remain highly dependent on androgen receptor signaling and therefore androgen

receptors still play an important role in CRPC, which lead to the progression of cancer cells. CRPC show high expression of androgen receptors, with the androgen receptor gene amplified. Prostate-specific antigen (PSA) is also coded by the genes involved in androgen receptor regulation.[2] Treatment of prostate adenocarcinoma is typically monitored by PSA levels returning to baseline, but when resistance develops, PSA levels begin to rise. Resistance typically occurs within 12 to 33 months after therapy begins.[41]

There are several theorized mechanism of actions for the development of CRPC, but the most widely excepted mechanisms include 1) androgen receptor activation by androgens derived from adrenal androgens or intratumorally synthesized, 2) androgen receptor hypersensitivity in prostate cancer cells due to overexpression of androgen receptor proteins (AR gene amplification) and 3) activation of androgen receptor signaling in prostate cancer cells due to an androgen receptor mutation or truncated androgen receptor, which lacks a ligand-binding domain (constitutive activation of androgen receptors).[1] The most common cause is believed to be the activation by adrenal androgens or intratumorally synthesized androgens. [42-52] LH-RH agonists only suppress testicular androgen synthesis and have no effect on adrenal androgen production, which is regulated by ACTH. Because of the limited therapies, effective treatments for CRPC is a pressing concern, as most patients succumb to the disease.[53]
Currently, CRPC is treated with radiopharmaceuticals, monoclonal antibody, immunotherapies, and chemotherapy, as well as antiandrogen agents such as abiraterone acetate and enzalutamide.[40] Pharmaceutical investigation of CRPC as led to the development of highly potent antiandrogen therapies, such as abiraterone acetate that blocks AR signaling via inhibition of hormone production.[1] Abiraterone acetate inhibits androgen receptor signaling, while enzalutamide is second-generation non-steroidal androgen antagonist. Unfortunately, both drugs have been shown to have limited durability, with the progression to Neuroendocrine Prostate Cancer (NEPC) occurring in most of the cases.[54, 55] The only chemotherapy agents that have shown to prolong the overall survival of CRPC patients is docetaxel, which reversibility stabilizes microtubule and inhibits cell division. Common side-effects of docetaxel include anemia, neutropenia, diarrhea and sensory neuropathy.[56]

2.2 Neuroendocrine Prostate Cancer

2.2.1 Overview of NEPC

Neuroendocrine Prostate Cancer (NEPC) is truly a unique medical condition, as it almost exclusively develops because of androgen deprivation treatment for prostate adenocarcinoma. NEPC rarely arises de novo, as the majority of NEPC patients are first diagnosed as prostate adenocarcinoma and treated with androgen deprivation therapy before evolving into NEPC.[1, 19] Approximately 87% of NEPC patients were first diagnosed with prostate adenocarcinoma and received anti-androgen treatment, which led to the term "treatment-related NEPC"(t-NEPC).[1] NEPC, also known as anaplastic prostate cancer or small-cell carcinoma of the prostate, is an aggressive form of prostate cancer with metastatic disease, which includes visceral sites.[19] While NEPC represents only approximately 2% of all prostate cancer cases, the incidence numbers are expected to rise dramatically as result of high potency antiandrogens, such as abiraterone acetate and MDV3100.[1, 57]

2.2.2 Clinical presentation of NEPC

NEPC patients typically do not respond to androgen deprivation therapy, but unfortunately, there is no current treatment for NEPC. Only about half of NEPC patients show a response to platinum-based chemotherapy but ultimately succumb to this devastating disease.[1] Since the prognosis is very poor once NEPC once diagnosed, the only mainstay treatment includes palliative care for the remainder of the patient's life, as patients only respond transiently to chemotherapy.[18, 58] Clinically, NEPC presents with as a rapidly progressing disease, involving visceral organs and proportionally low PSA.[19] Since PSA is lower than expected for the presentation of disease, PSA is a less accurate measure to diagnose, stage and monitor NEPC.[1] Therefore other serum markers are used to diagnose and monitor the progression of the disease, such as chromogranin (CgA), synaptophysin (SYP) and neuron-specific enolase (NSE), which are screened via IHC staining.[58]

The current chemotherapeutic regimen for NEPC patients includes a combination of either cisplatin, etoposide, carboplatin or docetaxel.[59] Docetaxel, which is also used in CRPC, reversibility stabilizes microtubule and inhibits cell division, while cisplatin, a platinum-based therapy, cross-links with purine bases of the DNA causing impaired DNA repair and results in DNA damage and apoptosis. Both show a 12-month median survival in NEPC patients. [56, 60] Etoposide inhibits DNA topoisomerase II from DNA re-ligation, which leads to inhibition of DNA synthesis and apoptosis of cancer cells. Carboplatin is an alkylating agent that also causes cross-linkage in DNA, which modifies the structure and inhibits DNA synthesis. Both show 10 to 19-months median survival in NEPC patients.[61] Along with Aurora kinase inhibitors, such as PHA-739358 and Danusertib, Olaparib is another novel treatment that can potentially be used in NEPC patients. Olaparib is a poly-ADP-ribose polymerase 1 (PARP1) inhibitor, whereby PARP interactions with ERG leading to DNA damage in ERG-positive cells. Since 50% of prostate adenocarcinoma and 44% of NEPC cases show ERG rearrangement, Olaparib has a potential for these patients.[62]

2.2.3 Pathophysiology of NEPC

NEPC is often confused with CRPC, since both lack response to androgen deprivation. As a result, more potent anti-androgens are used in NEPC, which causes further progression of the disease.[63] While approximately 20% of NEPC cases tend to develop from CRPC, most patients develop directly from prostate adenocarcinoma. Table 2.2 shows a comparison between NEPC and CRPC.[19] Metastasis for both NEPC and CRPC typically occurs via hematogenous spread, which includes visceral organs such as brain, lung, liver, bone and lymph nodes.[57]While both conditions show advanced metastasis, but the most common site for metastasis for NEPC tends to the liver, while CRPC tends to metastasize to the bone.[19] Typically, metastasis in NEPC is far more aggressive than CRPC, and as a result, NEPC is typically diagnosed in the setting of metastatic CRPC cases.[58, 64] Another key difference is the levels of serum PSA; while CRPC shows proportional levels compared to the progression of the disease, in NEPC, PSA levels are near normal levels, which is due to the lack of AR involvement. The final difference between CRPC and NEPC is the progression of the disease after androgen deprivation therapy. CRPC tends to develop over years of androgen deprivation

and is due to circulating androgens from the adrenal or produced from the tumor itself. But NEPC tends to progress in less than 12 months upon starting androgen deprivation therapy, presenting with distant metastasis. [65]

Table 2.2 NEPC vs. CRPC

	CRPC	NEPC
Bone Metastasis	Common	Maybe present
Liver Metastasis	Uncommon	Common
Brain Metastasis	Uncommon	Common
Serum PSA	Proportional to disease	low in proportion to disease
Hormonal Therapy Response	selective	no response
Serum Markers	PSA, AR, PSMA	synaptophysin and CgA
Progression after Androgen Deprivation Therapy	> 12 months	< 12 months

Approximately one-quarter of prostate mortalities show no dependence on the androgen receptor pathway. Androgen withdrawal seems to be a potent stimulus for prostatic neuroendocrine differentiation, with circulating cytokines contribution to the differentiation as well. But the mechanism by which this transformation from prostate adenocarcinoma or CRPC to NEPC is not yet completely known.[66] Similar to small cell carcinoma of the lung, NEPC shows a loss of retinoblastoma-related gene (RB2).[57] FISH has shown ERG rearrangement in NEPC cells, as well as Aurora kinase A (AURKA), and n-MYC (MYCN) amplification. Approximately 56-68% of NEPC cell lines (22rv1 and LnCAP) show an overexpression of n-MYC.[18] While NEPC shows little no androgen receptor expression, it shows TMPRSS2-ERG gene fusion in 44% of cases, which is similar to the approximately 50% found in prostate adenocarcinoma.[18, 19, 67] These fluorescence probes have also shown the TMPRSS2-ERG, AURKA and MYCN in liver and lung metastasis, which attributes the origin to the prostate.[58, 67] Aurora kinase A, a cell cycle kinase, is stabilized by the MYCN, which is a proven cancer driver or oncogene. AURKA is a serine-threonine kinase that is involved in cell division, specifically mitotic spindle formation, centrosome separation and G2-M transition.[18, 19] *In vitro* and *in vivo* studies have shown the effectiveness of Aurora kinase inhibitors, such as PHA-739358 and Danusertib, in NEPC models (LNCaP model) and currently, there are clinical trials for several potential agents. PHA-739358 is currently in phase II which has shown clinical benefits in patients with

overexpression of AURKA and MYCN.[18] MYCN is a transcription factor involved in nerve development, which is not expressed in prostate adenocarcinoma. [68]

When comparing benign prostate tissue with NEPC and prostate adenocarcinoma, IHC showed that AURKA and MYCN were overexpressed in 0% of benign prostate cases, while expressed in 12% and 4% respectively in prostate adenocarcinoma.[18] This is significantly lower when compared to 76% AURKA and 40% MYCN with regards to overexpression in NEPC. But over 90% of NEPC show concurrent amplification of AURKA and MYCN together.[18] As it seems, overexpression of AURKA and MYCN seem to go hand in hand with each other.

The World Health Organization (WHO) classifies NEPC differentiation into 5 subtypes in 2016: small-cell neuroendocrine carcinoma, large-cell neuroendocrine carcinoma, adenocarcinoma with neuroendocrine differentiation, adenocarcinoma with Paneth cell-like neuroendocrine differentiation and well-differentiated neuroendocrine tumor (carcinoid tumor).[19, 57] Histologically, NEPC differs from prostate adenocarcinoma. The most common subtype of NEPC is the small-cell carcinoma, which exhibits small, round, blue neuroendocrine cells and does not express androgen receptors.[18] Small cells typically have absent nucleoli, scant cytoplasm, ill-defined borders and finely granular chromatin.[57] The neuroendocrine tumor arises from hormone-secreting cells, such as secretory glands of the prostate, and are made up of a combination of endocrine and nerve cells.[69]

2.2.4 MYCN in NEPC

While MYCN is a transcription factor involved in nerve development[68], its' targets also include expression of Aurora kinase A and acts on down-stream markers of AURKA.[70] Chromatin immunoprecipitation (ChIP) analysis in LNCaP cells, which phenotypically resemble NEPC, showed MYCN does not bind to the promoter side for AURKA but binds to the E-box elements associated with MYCN-responsive promoters for telomerase reverse transcriptase (hTERT). It appears the MYCN protein physically provides stability to the AURKA protein via direct protein-protein interaction.[71] Chromatin immunoprecipitation shows that in Neuroblastoma, MYC binds to the promoter sites for NSE and SYP, but not the androgen

receptor promotor site. Also in neuroblastoma, there seems to be a positive feedback loop in which AURKA induces MYCN.[68] But the LNCaP model also showed overexpression of MYCN and the upregulation of NSE, an NEPC serum marker, as well as the downregulation of androgen receptors and TMPRSS2, an androgen-regulated gene.[18] As a result, LNCaP overexpressing MYCN phenotypically resembles NEPC. MYCN is commonly amplified in neuroendocrine tumors, including neuroblastoma, other central nervous system tumors, and small cell lung cancer.[72] In neuroblastoma, another highly aggressive neuroendocrine tumor, AURKA interacts with the oncogene MYCN independent of its role in mitosis. [18]

2.3 MYCN

MYC is primarily involved in embryogenesis and is also elevated in highly proliferative tissue, such as the skin epidermis.[73] MYC is a master regulator, controlling several processes, which include cell cycle, metabolism, signal transduction, apoptosis, ribosome biogenesis, RNA polymerase II and maintenance of pluripotency. But it is still not fully understood how MYC accomplishes these regulatory functions.[74, 75] Pluripotency is the ability of a cells to develop into 3 primary germ layers; ectoderm, mesoderm or endoderm. The ectoderm is responsible for the nervous system and sensory epithelia, while the mesoderm gives rise to connective tissue, muscle, kidneys, adrenals, and gonads. The endoderm is responsible for epithelial lines for the gastrointestinal, genitourinary and respiratory tract, as well as the epithelial line in the auditory system and several secretory organs.[74] But before its' role in pluripotency, MYC was known as an oncogene as it was first identified in leukemia cell lines in 1982. [76]

The MYC gene encodes for transcription factors that consist of MYC (c-MYC), MYCN (n-MYC) and MYCL (l-MYC). These transcription factors share a similar structure, which includes an amino-terminal (N-terminal) that contains the transcription activation domain. The carboxyl-terminal (C-terminal) contains a basic helix-loop-helix leucine zipper (bHLH-LZ) domain.[73] The bHLH-LZ region is involved in heterodimerization with MYC-associated factor (MAX) and consequently allows MYC to recognize the Enhancer box (E-box), which consist of the sequence CACGTG. The MYC-MAX heterodimer is essential for gene transcription, cell proliferation, apoptosis, and transformation.[73] Since MYC transcription factors share a similar structure,

they also share similar oncogenic properties, but roles seem tissue specific. [77] Knockdown studies have shown that c-MYC and n-MYC are functionally the same, and both are essential for early development, as well as directly implicated in transcriptional regulation.[78, 79]

In malignancy, the MYC network is often deregulated, which can occur via different modes. The most common mode for MYC deregulation is via gene amplification, whereby gene duplication occurs through genome doubling. This mode of deregulation occurs in multiple types of cancers, such as breast, gynecological, lung, and neuroendocrine tumors.[75] Deregulation of MYC is a hallmark of cancers associated with poor prognosis, with deregulated c-MYC associated with most human cancers and n-MYC associated with cancers arising from the neural system.[73] Cells that overexpress MYC also exhibit cancer-stem-cell traits, which enables cells to increase metastatic potential, while *in vivo* inactivation of MYC leads to tumor regression and loss of neoplastic phenotypes.[73] Deregulation of MYC may trigger chromosomal instability, while it may also lead to uncontrolled activation of downstream genes that promote cell cycle and DNA synthesis. [80, 81]

The MYC transcriptional factors are all associated with cancers, but n-MYC and c-MYC are more characterized by their proto-oncogenic properties as compared to l-MYC. MYCN was first reported in 1983 with its' association in neuroblastoma, a highly aggressive neuroendocrine tumor that is the most common pediatric extracranial solid tumor.[82] While neuroblastoma was the first tumor associated with MYCN, with 20% of cases showing amplification of MYCN, other tumors have now been shown to have an association with MYCN. Table 2.3 lists the top cancers associated with MYCN amplification, and as can be seen, NEPC ranks among the highest, with 40% of cases showing MYCN amplification.[77]

Table 2.3 Summary of n-MYC (MYCN) Associated Tumors

Tumors types	Frequency of MYCN Amplification	Prognosis
NEPC	40%	Poor
Triple Negative Breast Cancer	40%	Poor
Neuroblastoma	20%	Poor
Alveolar Rhabdomyosarcoma	25%	Poor
Small-cell lung cancer	15-20%	Poor
Retinoblastoma	< 5%	Poor

n-MYC is coded by MYCN gene on chromosome 2 (2p24) and is important for cellular proliferation and growth, as well as apoptosis and energy metabolism.[77, 83] But n-MYC is typically expressed during embryogenesis, with the highest expression in the developing brain, driving the proliferation of neuron precursors.[77] Inactivation of MYCN can lead to a rare condition known as Feingold Syndrome, which is associated with microcephaly, gastrointestinal atresia, limb abnormalities and mental deficits.[84] After embryonic development, MYCN is typically downregulated in adult tissue, except in malignancies. MYCN is associated with neuroendocrine tumors, such as neuroblastoma and small-cell carcinomas, as well as neural system tumors, such as medulloblastoma and glioblastoma. c-MYC is pathognomonic for Burkitt's lymphoma but also found in cancers found in breast, colon, liver, as well as gynecological and hematological cancers.[77] There is a growing importance in oncology for these molecular aberrations to create personalized treatments, by linking molecular aberration in tumors with therapeutics.

2.4 High-Throughput Screens

Traditionally, new therapeutic compounds development can take several years before they reach patients, and require an enormous amount of investment. The average length for development takes approximately 10 to 12 years and can require millions in resources.[85] The rate-limiting step in drug discovery has always been the extensive protocols that clinical trials entail. Phase 1 typically lasts for 12 months and begins with a small patient population, with drug safety the primary research outcome. Approximately 70% pharmaceutical agents move onto phase 2 and 33% eventually move onto phase 3; both phase 2 and 3 try to identify drug efficacy and adverse side-effects. Test groups are typically in the hundreds to thousands and can last several years. Phase 4 is the final stage, which looks at disease-specific situations for optimization.[86] Therefore, novel drug discovery is limited to the in-depth and extensive process associated with clinical trials.

While the use of high-throughput screen is not a novel idea, the clinical usefulness for repurposing has only recently been realized. Drug repurposing has a viable alternative for rapid

identification of effective therapeutics, specifically in drug-resistant conditions. High-throughput screening can accommodate a large number of compounds, and specifically looking at FDA approved compounds can identify drugs for repurposing as well as combinations that lead to synergistic drug combinations.[87]

The goal of most pharmaceutical companies is to find 'blockbuster drugs', which are developed for disorders that impact a large population and can earn at least $1 billion in annual returns.[87] But orphan drugs that are developed to treat less rare disease, offer less financial returns and as a result, offer fewer incentives for development.[87] Drug repurposing afters an alternative, as there are far less financial costs, as the majority of the investment was done during development.

Over the last decade, the cytotoxic chemotherapy, with its' one-size-fits-all approach, has transitioned to molecularly targeted cancer drugs that allow for a personalized medicine strategy. This strategy focuses on genetic or molecular alterations, which may lead to targets for cancer vulnerability, and these exploitable characteristics have been accelerated by genome sequencing and high-throughput screens.[88] Personalized therapy is not a new idea, as anti-estrogens for breast cancer and anti-androgens for prostate cancer have long been employed, but despite the progress in molecular targeted chemotherapy, significant challenges still present itself for new drug discovery. The first challenge is to recognize a specific oncogene target that has a potential for drug action. But sequencing has shown complexity and heterogenicity, not only between tumors but within individual cancers themselves.[88, 89] This can lead to a "druggability gap", whereby promising targets are untreatable by chemotherapy due to heterogenicity of tumor or essential action of the targets. Along with these biological challenges, technical issues arise from transitioning from *in vivo* and *in vitro* models to clinical models.[88] But despite these challenges, personalized molecular therapy for patients is the ultimate goal of chemotherapy.

Discovering personalized therapy in oncology involves 4 steps. The first and most crucial step is identifying a molecular target because once a target has been chosen, a considerable amount of time and resources are used to test the target. [88] Selecting the right target is based on both the opportunity to find a novel drug and the risk that target will not translate to therapeutic effects or lead to a therapeutic agent. The next step involves finding a chemical hit, which is based on 2

different approaches; knowledge-based versus random. In knowledge-based screens, prior knowledge of the target by either crystal structure or known inhibitors or natural ligands is required, and screens typically test a small number of compounds. In comparison, random screens do not require prior knowledge and are unbiased in identifying novel compounds, and test many compounds.[88, 90] Virtual screening is based on selecting potential targets from large databases that contain information about ligand-binding or structure, and these screens are typically done a few hundred compounds. Fragment screening focuses on a limited number of small molecules that a relatively low concentration, and therefore addressing one key challenge of high-throughput screens; sufficient potency for potential hits. Random-non-focused screens focus on screening a large number of compounds in order to identify compounds that induce a particular phenotype or inhibit proliferation or survival of cancer cells.[88] Typically, random-non-focused screens are done when little knowledge is known about a potential target. While little is known about MYCN mechanism of action, it is well-defined as a potent oncogene and associated with poor prognosis. Also, finding these potential agents that exhibit chemical selectivity for molecular alterations is key for conditions like NEPC, which does not have known therapeutic agents. Therefore, NEPC is an ideal model for a large random screen with small molecules, since NEPC expresses a known oncogene in MYCN, which is not expressed in adult tissue.

2.5 Targetmol Drug Library

The Targetmol Drug Library is composed of 1813 small molecules; 1105 FDA approved, 687 approved and 21 withdrawn small molecules. There are approximately 2700 FDA approved compounds clinically available in the United States[91]. The approved compounds are clinically used outside of the United States. The withdrawn small molecules were previously used in the United States, but have been replaced due to advancements in treatment options or severe adverse effects.

Figure 2.6 illustrates the FDA approved small molecules, which target variety of biological systems. Immunology is the most common system with 30% of small molecule agents. Oncology

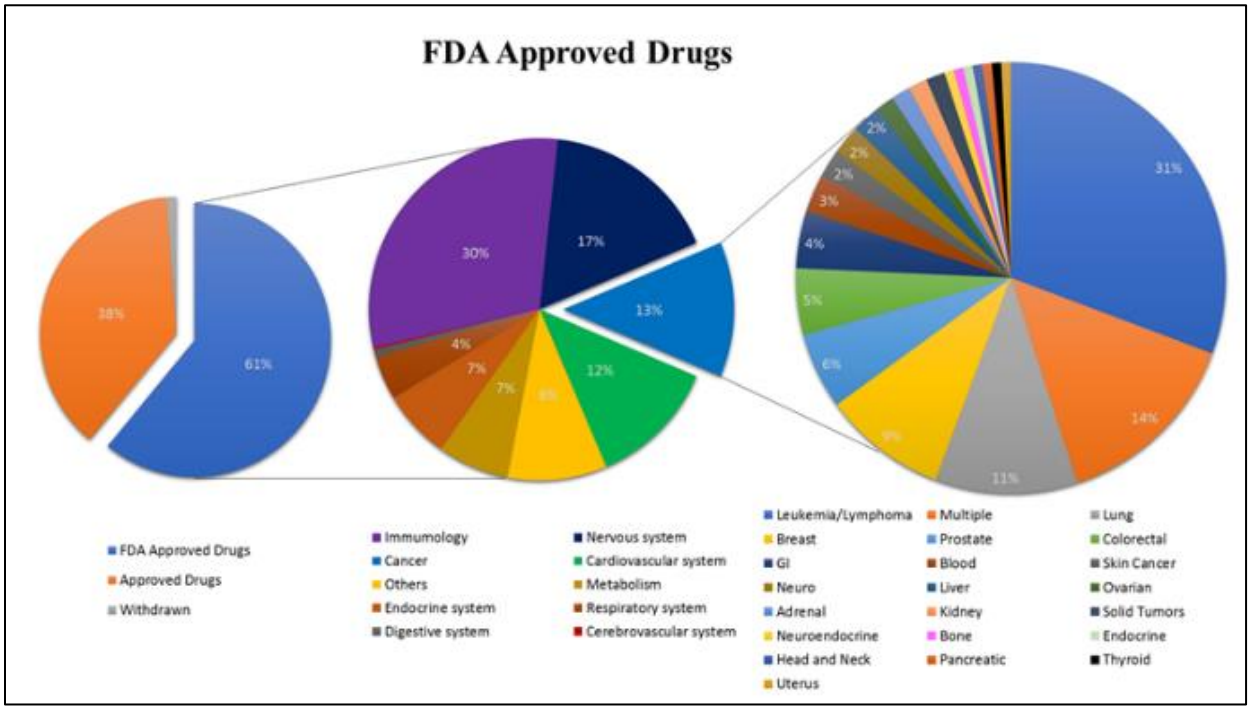

Figure 2.6 Targetmol Drug Library FDA Approved Small Molecules. FDA approved small molecular account for the majority of the Drug Library.

related compounds represent 13% of the FDA approved small molecules, and target several types of cancers, with agents for leukemia and lymphomas being the most common. Figure 2.7 illustrates the mechanism of action for FDA approved anticancer drugs, and the most common mechanism of action for FDA approved cancer drugs are agents that target DNA/RNA synthesis.

The approved drug library represents a smaller portion of the drug library, but still targets a variety of biological systems. Figure 2.8a illustrates the Targetmol approved drug library, with immunology again representing the largest area targeted. Oncology related compounds represent 8% of the approved drug library, but unlike the FDA approved library, most of the anti-cancer approved drugs target multiple oncology conditions. While these agents are not clinically used in the United States, several are currently in clinical trials. Figure 2.8b illustrates the small molecules that are currently in clinical trials, with approximately 50 compounds currently involves in various stages, some of which in multiple stages.

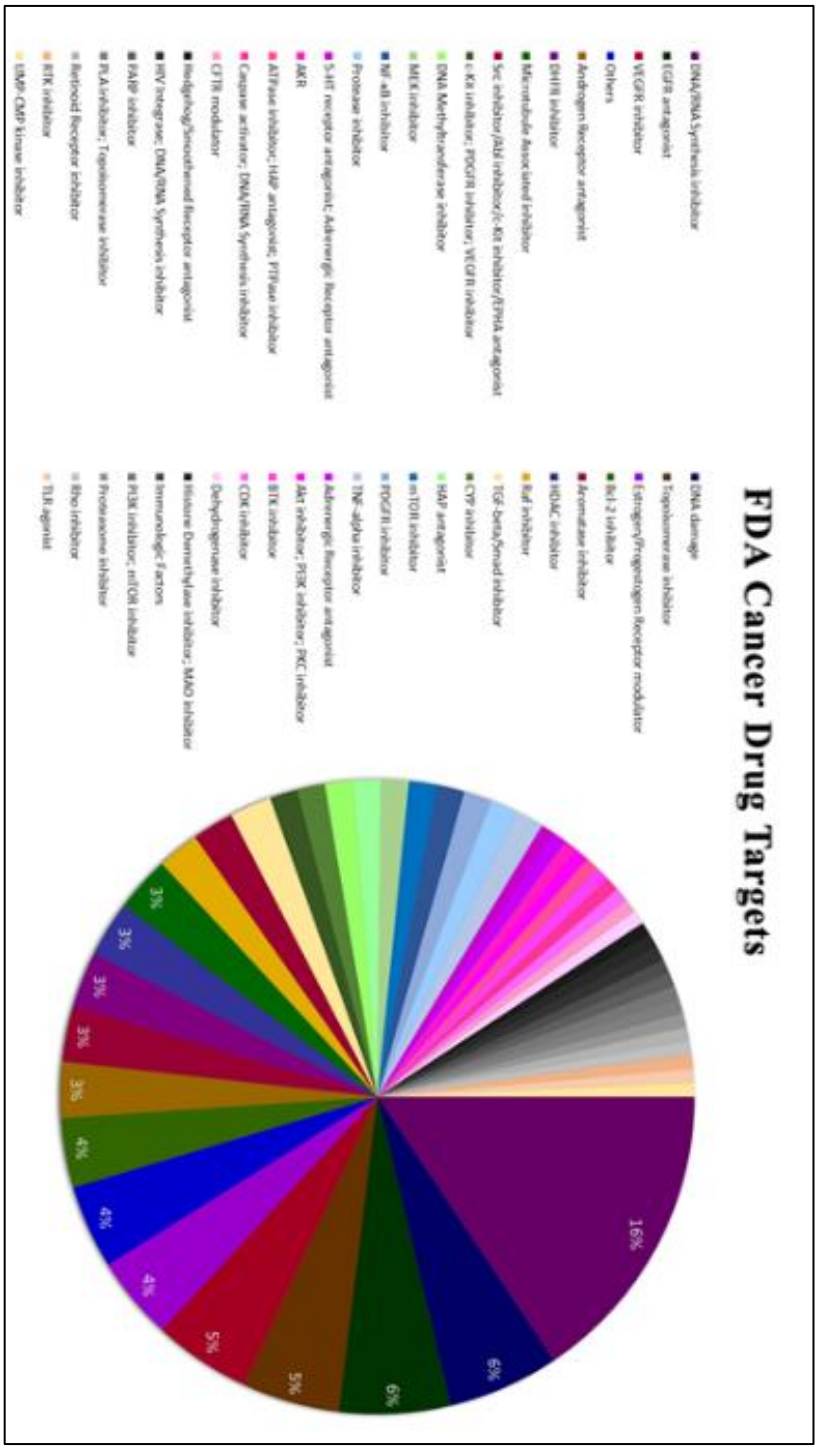

Figure 2.7 Targetmol Drug Library FDA Approved anticancer drugs. Small molecules target a variety of mechanisms, with DNA/RNA synthesis inhibitors as the most common.

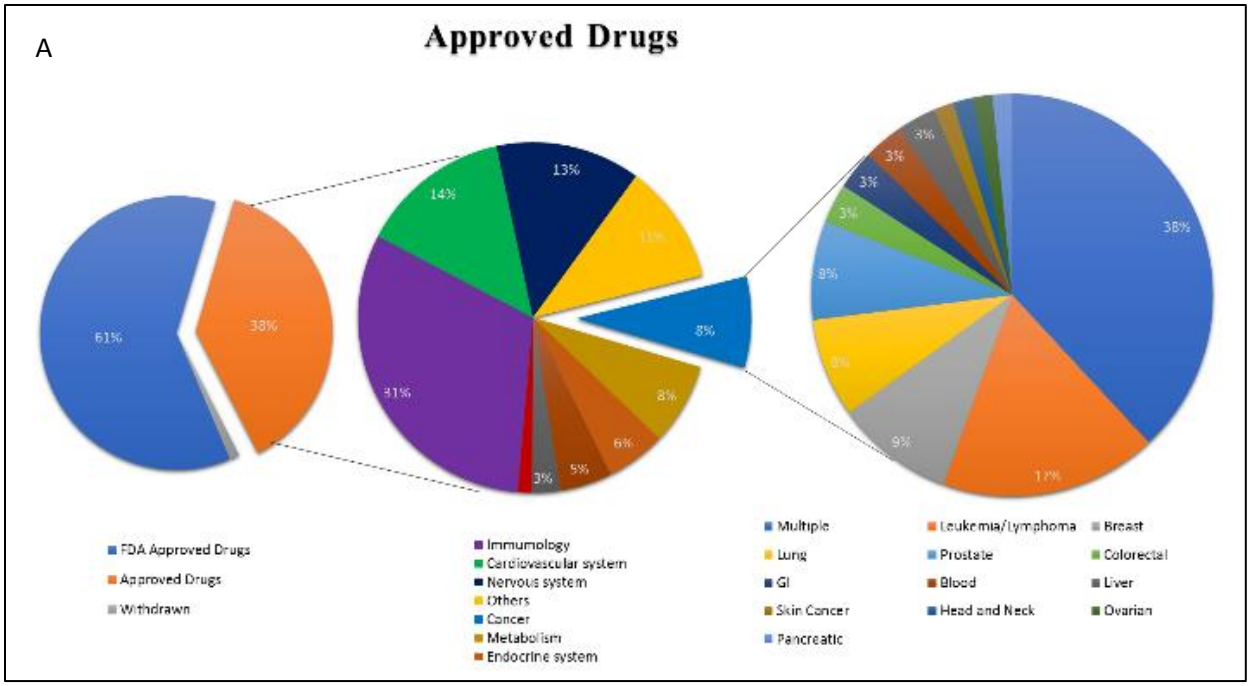

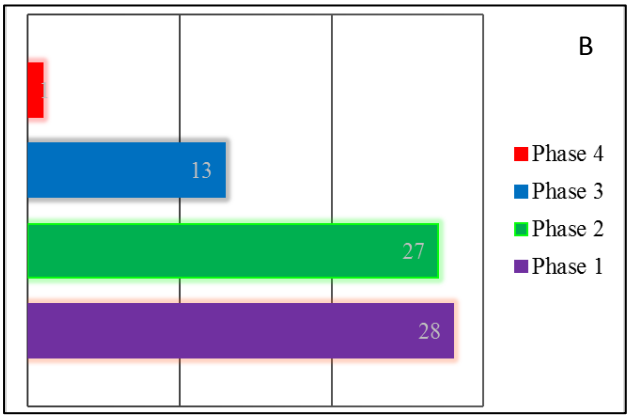

Figure 2.8. A) Targetmol Drug Library Approved Small Molecules. Approved small molecular account for the majority of the Drug Library. B) Approximately 50 small molecules from the approved drug library are currently in various stages of clinical trials in the United States.

3. Methodology

3.1 Cell Lines and Culture Conditions

LnCAP-P, LnCAP-N-MYC, 22RV1-P, 22RV1-N-MYC and BPH-1 cell lines (were kindly provided by the Rickman Lab from Cornell Medical College) and were grown in RPMI 1640 (Hyclone, #SH30027.01) containing 10% Fetal Bovine Serum (Hyclone, #F1051) supplemented with 1% penicillin/streptomycin (Hyclone, #SV30010). HEK293T cells were cultured in DMEM (Hyclone, #SH30243.01) containing 10% Fetal Bovine Serum (Hyclone, #F1051) supplemented with 1% penicillin/streptomycin (Hyclone,#SV30010).

3.2 Western Blotting

Total cell lysates were prepared using RIPA buffer (Pierce,#89901). Protein lysates were quantitated using BCA assay (Pierce, #23225). Equal amounts of protein were loaded onto a 10% SDS-PAGE gel and resolved by electrophoresis in Laemelli buffer. Protein from gels was transferred on to a PVDF membrane (#162-0177) using wet transfer 20% methanol. Blots were rinsed with 1X TBS-T and blocked for 1h at RT in 5% milk diluted in 1X TBS-T. Blots were incubated with primary antibody for GAPDH (#SC-25778) and N-MYC (#SC-53993) overnight at 4°C. Blots were washed 3 times for 5 min each followed by a 2h incubation at room temperature with secondary antibody conjugated with HRP rabbit secondary antibody (#31460) and HRP mouse secondary antibody (#31430). Blots were washed for 3 times for 10 min each then incubated with Clarity™ Western ECL Substrate (#170-5060) and imaged using a BioRad ChemiDoc™ MP Imaging System.

3.3 RT-qPCR

Total RNA was extracted from cells as per manufactures via Qiagen RNeasy Mini Kit (#74104) and QIAshredder (Qiagen, #79654), which was used for cell homogenization. The conversion to cDNA was done using applied Biosystems Kit (#4368814) as per manufactures instructions.

DNA digestion was not because the RNeasy mini kit, which is a component of the Qiagen kit, yields a high amount of RNA, with only trace amounts of DNA. cDNA was mixed with Applied Biosystems TaqMan master mix (#4369016) and TaqMan primers to MYCN (#hs00232074_m1 MYCN FAM) and GAPDH (hs02758991_g1 GAPDH VIC), which was run on applied BioSystems StepOne Pluse® Real-Time PCR System. OD (optical density) readings were assessed to ensure the sample only contained pure RNA rather DNA. Expression Fold Change is determined by 2 to the exponent of negative ΔΔCt, since all calculates are in logarithm base 2. ΔCt is calculated by taking the average Ct value of MYCN minus average Cr value of GAPDH in each of the cell lines (BPH-1 vs. LnCAP-n-MYC, BPH-1 v. 22rv1-n-MYC, LnCAP-P vs. LnCAP-n-MYC and 22rv1-P vs. 22rv1-n-MYC). Ct values represent the basic result of a qPCR, which is defined as the number of cycles required for a signal to cross the threshold of the background level. ΔΔCt is calculated by taking the difference between experimental group (LnCAP-n-MYC and 22rv1-n-MYC, respectively) from the control groups (BPH-1, LnCAP-P, and 22rv1-P).[92]

3.4 Lentivirus Propagation and Lentiviral Transduction

HEK293T packaging cells were plated at a density of 3 x10^5 cells/well in 6 well plates 24h prior to transfection with psPAX2.2, pMD2.6, PL-RFP-hygro (Vizeacoumar et al, 2013). 24h post-transfection media was removed and replaced with viral harvest media DMEM containing 1.1 % BSA, 1% penicillin/streptomycin. Media was collected at 48h and 72h post-transfection, pooled and used for transduction. The remaining virus was aliquoted and stored at -80°C.

3.5 Stable Clones Expressing RFP

Stable clones of LnCAP-P and LnCAP-N-MYC were made by transducing cells with lentivirus-PL-RFP-hygro (Vizeacoumar et al, 2013). The selection was done using 50ug/ml hygromycin (Invitrogen#10687010) for 5 days to make stable cell lines expressing RFP. Images were taken upon completion of the selection with Evos® FL Color Imaging System (#AMEFC4300). Figure

3.1 illustrates BPH-1-RFP images, with image to the left without RFP filter and image to the right with RFP filter.

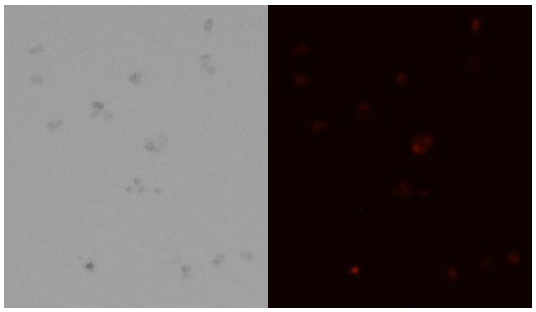

Figure 3.1 BPH-1-RFP. A) Image taken without filter. B) Image taken with RFP filter.

Figure 3.2 illustrates LnCAP-P-RFP images, with image to the left without RFP filter and image to the right with RFP filter.

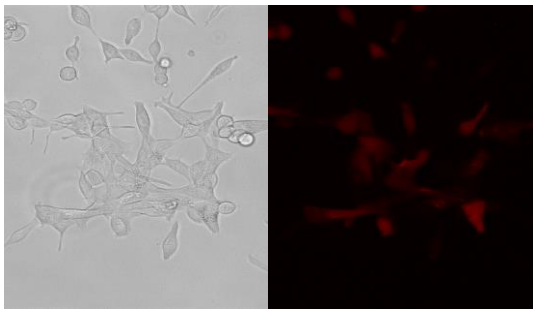

Figure 3.2. LnCAP-P-RFP. A) Image taken without filter. B) Image taken with RFP filter.

Figure 3.3 illustrates LnCAP-n-MYC-RFP images, with image to the left without RFP filter and image to the right with RFP filter.

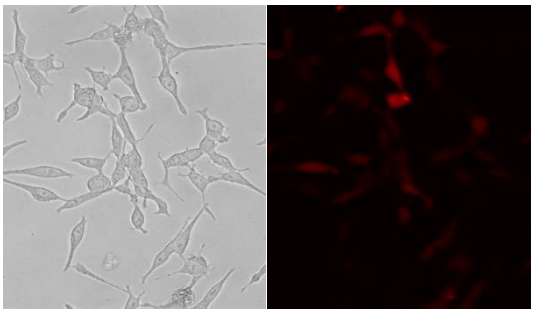

Figure 3.3. LnCAP-n-MYC-RFP. A) Image taken without filter. B) Image taken with RFP filter.

3.6 Drug Screen

3.6.1 Dilution of Targetmol Drug Library

Targetmol Drug Library Stock concentration was 10 mM per Drug in DMSO. Each drug was diluted into 384-well plates to target concentrations with Dimethyl Sulfoxide (Fisher BioReagents #L-15579) as per Targetmol instructions. 2.5 µL of 10 mM was combined with 47.5 µL of Dimethyl Sulfoxide (Fisher BioReagents #L-15579) to yield 50 µL of 500 µM per drug plates. Then 16.25 µL of 500 µM was combined with 16.25 µL of Dimethyl Sulfoxide (Fisher BioReagents #L-15579) to yield 32.5 µL of 250 µM per drug plates. Then 12.5 µL of 250 µM was combined with 12.5 µL of Dimethyl Sulfoxide (Fisher BioReagents #L-15579) to yield 25 µL of 125 µM per drug plates. Finally, 5 µL of 125 µM was combined with 20 µL of Dimethyl Sulfoxide (Fisher BioReagents #L-15579) to yield 25 uL of 25 µM. Plates sealing film was used to seal the 24 plates (6 plates per concentration) and plates were stored at -20^{o}C. Target concentration after 200 nL dispensed from plates are: 2000 nM, 1000 nM, 500 nM and 100 nM.

3.6.2 Robotic Seeding of BPH-1 and LnCAP cell lines

BPH-1-RFP, LnCAP-P-RFP, and LnCAP-MYCN-RFP were counted using Countess™ II Automated Cell Counter (#AMQAX1000) and cell lines were plated at a density of 300 cell/well in 50 µL of in RPMI 1640 (Hyclone, #SH30027.01) containing 10% Fetal Bovine Serum (Hyclone, #F1051) supplemented with 1% penicillin/streptomycin (Hyclone, #SV30010). Each cell line was plated in 6 384-well Imaging plates (#142761) using a BioMek NX liquid handling robot. Figure 3.4 illustrates seeding distribution from BioMek NX liquid handling robot. Cell count was assessed via Molecular Devices XLS non-confocal high-throughput prior to treatment with Targetmol Drug Library. Cell distribution found 95% of wells were plated within 15% of

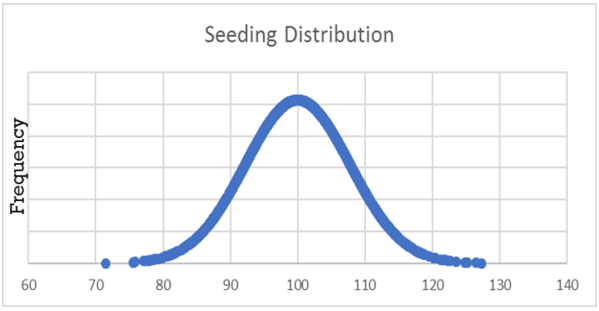

Figure 3.4. Robotic Seeding Distribution Curve. Cell count was normally distributed among all wells.

mean of all wells, which was congruent with the high degree of accuracy expected from automated liquid handling robots.

3.6.3 Drug Pinning of Targetmol Drug Library

Drug pinning tool by V&P Scientific was used by BioMek NX liquid handling robot to dispense 200 nL from drug plate to 384-well Imaging plates (#142761) containing each cell line; BPH-1-RFP, LnCAP-P-RFP and LnCAP-MYCN-RFP. Drug pinning tool by V&P Scientific was cleaned prior to each cell line treatment by washing in double distilled water, then drying with lint-free drying paper, then washing with 100% ethanol and finally drying again with another piece of lint-free drying paper. Drugs were dispensed 96 wells at a time, with cleaning protocol with double distilled water and 100% ethanol was done between dispensing.

3.6.4 High-Throughput Non-Confocal Microscope Imaging

BPH-1-RFP, LnCAP-P-RFP, and LnCAP-MYCN-RFP were plated at a density of 300 cell/well in 384-well Imaging plates (#142761) and plates were imaged using non-confocal high-throughput microscope by Molecular Devices. The benefits of using high-throughput imaging allowed for detection of the onset of action as well as the duration of action via monitoring cell count.

Images were taken at 4x magnification, with 4 images taken per well. Automated cell counts were assessed via MetaExpress software with Texas Red filter and count was optimized via digital and manual count. Figure 3.5 illustrates high-throughput non-confocal image seen in MetaExpress software. Left side shows image with red fluorescence expressed cells, while the right side shows the image with the blue overlay that corresponds to the cell count.

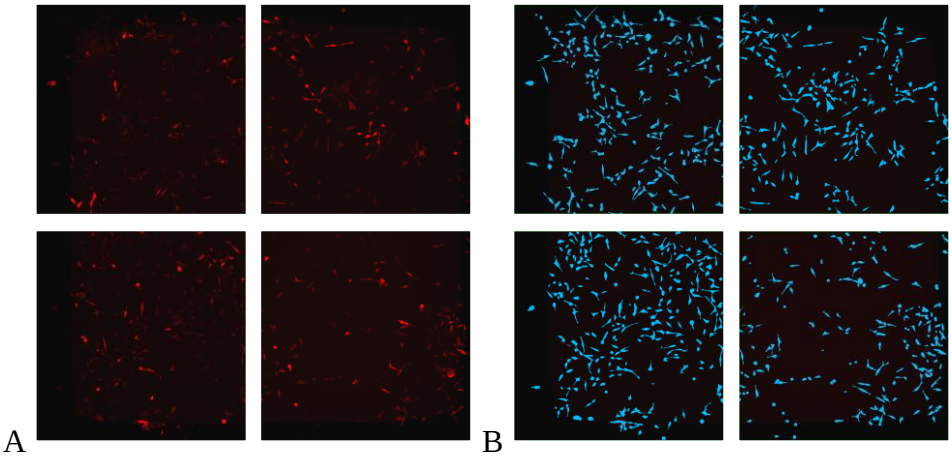

Figure 3.5. A) Images taken with Molecular Devices non-confocal microscope and viewed with MetaExpress software. B) Blue overlay counting cells that express RFP.

The drugs were added 24hrs after seeding, to ensure cell attachment and that cells open. 384-well Imaging plates (#142761) were imaged prior to drug pinning and for 5 consecutive days using a non-confocal high-throughput microscope (Molecular Devices). Cell counts were given by MetaExpress software and 1813 drug library was controlled using Dimethyl Sulfoxide wells.

3.7 Computational Scoring of Drug Library Screen

3.7.1 Statistical Analysis

Growth inhibition was determined by adjusting cell count by average DMSO cell count and then dividing by cell count prior to drug dosage, which presented as a percentage.

The assumption of homoscedasticity assumes equal variance among random variables, where variance is the spread of data from the mean and residuals difference from the mean. Homoscedasticity presents with a randomize scatter with no discernible pattern, while heteroscedasticity shows a pattern distribution of data points.[93]

3.7.2 B-score Analysis

B-scores are like Z scores, whereby they are a ratio of adjusted raw value to measure of variability. The adjusted raw value accounts for positional effects as well as plate-to-plate

changes in the means, while the variability is a resistant measure of the residual variability in the plate after plates are fitted by median polish by using median absolute deviation for the plate (MAD_p). The residual (r_{ijp}) is calculated by the difference between observed results and fitted value. The fitted value is the sum of the estimated average of the plate, measurement offset of row *i* on plate *p* and measurement offset of column *j* on plate *p*. MAD_p is an estimate of the spread of residual values (r_{ijp}).[93, 94]

$$\text{B-score} = \text{residual } (r_{ijp}) / MAD_p$$

3.8 Validation and Dose-Response Curve

Fludarabine Phosphate (#S1229) was reconstituted via Selleckchem instructions and serial concentrations of were made; 12800 nM, 6400 nM, 3200 nM, 1600 nM, 800 nM, 400 nM, 200 nM, 100 nM, 50 nM and 25 nM.

First, BPH-1, LnCAP-P, LnCAP-MYCN, 22rv1-P, and 22rv1-MYCN were plated at a density of 500 cells per well in 96 well plates, with 5 technical replicates per biological replicate (total of 3 biological replicates were done). 24h after seeding drug was added at the following concentrations: 25 nM, 50 nM, 100 nM, 200 nM, 400 nM, 800 nM, 1600 nM, 3200 nM, 6400 nM and 12800 nM. Alamar Blue™ Cell Viability Reagent (Invitrogen #DAL1100) was added at a volume of 10 ul to each well and readings using a SpectraMax MS spectrophotometer were done at 96h, and 120h after incubation. Percentage viability was calculated via the ratio of final fluorescence to OD reading compared, considering DMSO and media.

Step 1: Fluorescence value / OD value = individual relative % viability
Step 2: 100 x (individual relative % viability - average media alone Fluorescence/OD) / (average DMSO Fluorescence/OD - average media alone Fluorescence/OD)
Step 3: average of 10 replicates (2 biological replicates x 5 technical replicates) per concentration.

The sigmoidal curve was generated using GraphPad Prism, which determined the dose-response curve and IC50 values. Data for the dose-response curve was attained from the validation using Alamar Blue™ Cell Viability Reagent (Invitrogen #DAL1100).

4. Results

4.1 MYCN

The first goal was to see if there was a difference in MYCN expression between BPH-1, LnCAP-P, and LnCAP-n-MYC, as well BPH-1, 22rv1-P and 22rv1-n-MYC. To test this hypothesis, western blot and RT-qPCR was done. In western blots, cell lysates are quantified to determine protein concentration and compared to the positive and negative control (n-MYC and GAPDH). The results from the western is semi-quantitative, as it compares relative protein levels between the 3 test groups (BPH-1/LnCAP-P/LnCAP-n-MYC and BPH-1/22rv1-P/22rv1-n-MYC). To quantify MYCN expression, RT-qPCR was then completed. In RT-qPCR, RNA is transcribed into cDNA via reverse transcriptase, which is quantified and used for the qPCR reaction to determine. The RT-qPCR determines how much specific mRNA was found in the samples (BPH-1/LnCAP-P/LnCAP-n-MYC and BPH-1/LnCAP-P/LnCAPn-MYC).

Western Blot and RT-qPCR for BPH-1, LnCAP-P and LnCAP-n-MYC

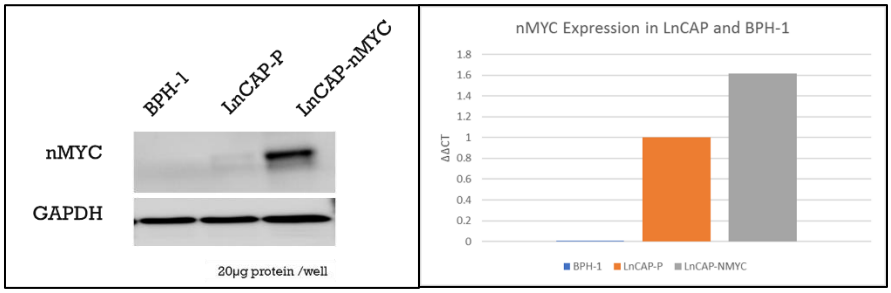

Figure 4.1. A) Western Blot for BPH-1, LnCAP-P and LnCAP-n-MYC. B) RT-qPCR for BPH-1, LnCAP-P and LnCAP-n-MYC.

Figure 4.1 illustrates the western blot, which was completed by Kalpana Kalyanasundaram Bhanumathy, and the RT-qPCR for BPH-1, LnCAP-P, and LnCAP-n-MYC. The western blot clearly shows a higher MYCN expression in LnCAP-n-MYC compared to BPH-1 and LnCAP-P,

while the RT-qPCR also showed higher expression of MYCN in LnCAP-n-MYC compared to BPH-1 and LnCAP-P. But the RT-qPCR also showed some expression of MYCN in LnCAP-P that wasn't detected by the Western blot. These results correspond to existing literature on MYCN expression in LnCAP.[18] Therefore, LnCAP-n-MYC can be used as a model to represent a cancer model that shows overexpression of MYCN, with BPH-1 and LnCAP-P representing controls (non-cancer and cancer control, respectively).

Figure 4.2 illustrates the western blot, which was completed by Kalpana Kalyanasundaram Bhanumathy, and the RT-qPCR for BPH-1, 22rv1-P, and 22rv1-n-MYC. The western blot clearly shows a higher MYCN expression in 22rv1-n-MYC compared to BPH-1 and 22rv1-P, while the RT-qPCR also showed higher expression of MYCN in 22rv1-n-MYC compared to BPH-1 and 22rv1-P. But unlike the LnCAP model, the RT-qPCR did not show expression of MYCN in 22rv1-P. Therefore, 22rv1-n-MYC represents a cancer model that shows overexpression of MYCN, with BPH-1 and LnCAP-P representing controls (non-cancer and cancer control, respectively).

Western Blot and RT-qPCR for BPH-1, 22rv1-P and 22rv1-n-MYC

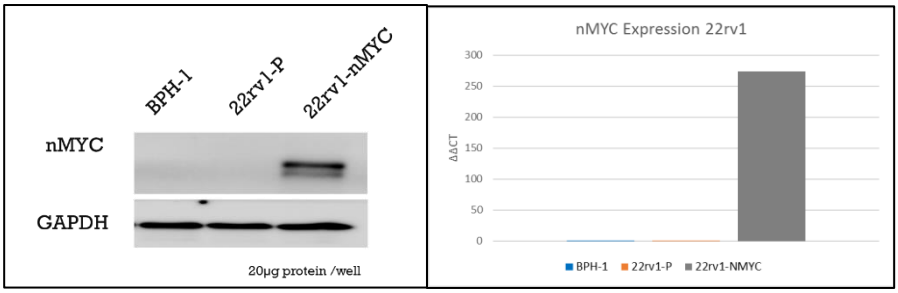

Figure 4.2. A) Western Blot for BPH-1, 22rv1-P and 22rv1-n-MYC. B) RT-qPCR for BPH-1, 22rv1-P and 22rv1-n-MYC.

4.2 Drug Screen of Targetmol Drug Library

The next goal was to see if there was a difference in cell count between BPH-1, LnCAP-P, and LnCAP-n-MYC, after use of Targetmol drug library. First, cell lines were plated at 300 cells per well and imaged at 24 hours after seeding via non-confocal high-throughput microscope. For 100 nM drug screen, 200 nL of 25 µM of each small molecule was administered to cell lines in a 384-optic plate (#142761). Images were taken at 24, 48, 72, 96 and 120 hours post-treatment, and cell count was adjusted with the average cell count from the 107 DMSO wells. Growth

inhibition was then calculated via final cell count divided by initial cell count and presented as a percentage.

Table 4.1 illustrates the descriptive statistics from the 100 nM drug screen, which displays a lower average mean score for LnCAP compared to BPH-1; Parental (90.4), MYCN (96.3) and BPH-1(100.9). Therefore, LnCAP-P and LnCAP-n-MYC showed a lower final cell count compared to BPH-1. But data also showed a negative skew with a high variance BPH-1, LnCAP-P, and LnCAP-MYCN; 1231.6, 902.1 and 562.8 respectively. The negative skew means that a larger proportion of the data was below the mean, which indicates either many drugs had a significant negative effect on the cells. From the data, LnCAP-n-MYC was the most sensitive to the drug library at 100 nM, showing the most number of wells below the mean, while LnCAP-P was the least sensitive to the drug library at 100 nM, showing the least number of wells below the mean. Interestingly, MYCN also showed the lowest variance (562.8) compared to the other 2 cell lines, which indicates the difference from the individual wells from the mean was the lowest in the MYCN cell line.

Table 4.1 Statistical analysis of 100 nM Targetmol Drug Screen BPH-1 and LnCAP

100 nM	**LNCaP-Parental**	**LNCaP-MYCN**	**BPH-1**
DMSO (# of wells)	107	107	107
Drug Library (# of wells)	1813	1813	1813
Mean Growth Inhibition	90.4045	96.3016	100.9155
Std. Error of Mean	0.68545	0.54142	0.80091
Std. Deviation	30.03502	23.72369	35.09432
Variance	902.102	562.814	1231.611
Skewness	-0.399	-1.387	-1.027
Std. Error of Skewness	0.056	0.056	0.056
Range	269.59	195.15	233.18
Minimum Growth Inhibition	-34.92	-20.37	-3.61
Maximum Growth Inhibition	234.66	174.78	229.57

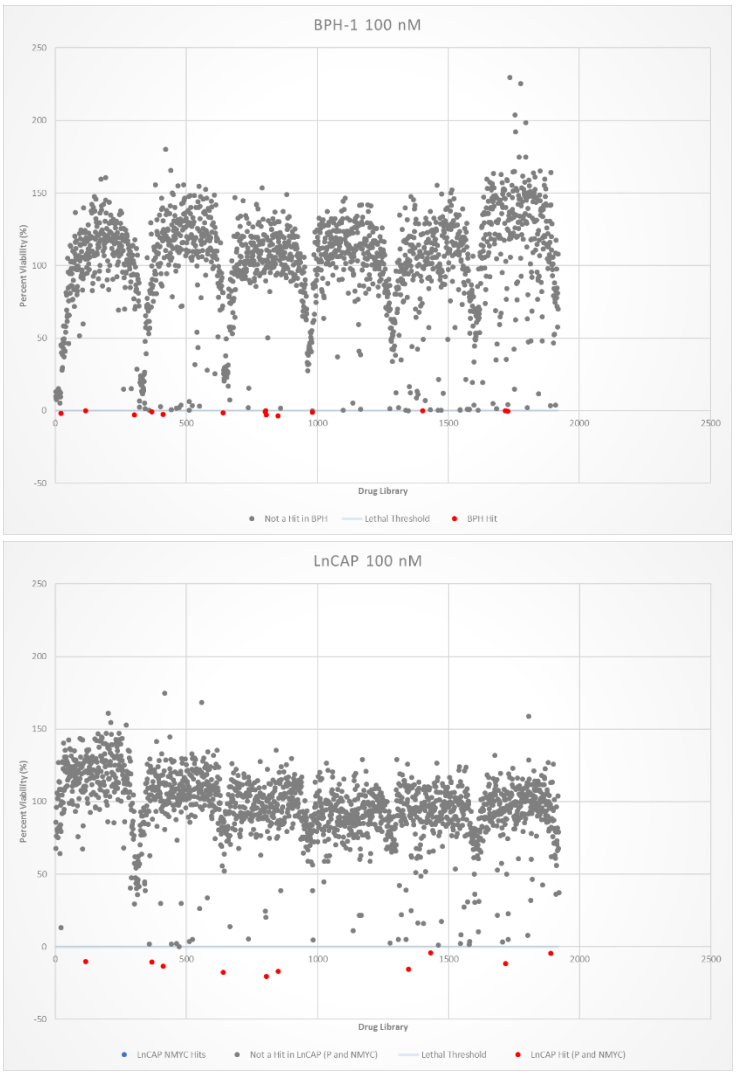

Figure 4.3. 100 nM 1813 Drug Screen Distribution. Cell count represent 120 hour post treatment. Cell count was controlled for DMSO. A) 100 nM screen in BPH-1. B) 100 nM screen in LnCAP.

Figure 4.3 illustrates the growth change from the 100 nM drug screen. In LnCAP, results between LnCAP-P and LnCAP-n-MYC were compared. The LnCAP-n-MYC results were below 0 are displayed as LnCAP-n-MYC hits and the LnCAP-P results below 0 are displayed as LnCAP-P hits. Non-LnCAP-P and non-LnCAP-n-MYC hits are values above 0 in both LnCAP-P and LnCAP-n-MYC, and Ln-CAP-P are displayed as Not a hit in LnCAP-P and LnCAP-n-MYC.

From Figure 4.3, several hits were seen in both BPH-1 and LnCAP-P at 100 nM, but no hits were seen in LnCAP-n-MYC. While several hits were seen, a pattern distribution of growth can be seen and reflect the plate distribution. There are 6 waves, which corresponds to the 6 plates

involved in the drug screen. Wells located near the edge of the plate show a lower average growth compared to the wells towards the middle of the plate. Therefore, 384-well plate exhibits cell susceptibility with regards to well location at the 100 nM dose concentration.

For 500 nM drug screen, 200 nL of 125 µM of each small molecule was administered to cell lines in a 384-optic plate (#142761). Images were taken at 24, 48, 72, 96 and 120 hours post-treatment, and cell count was adjusted with the average cell count from the 107 DMSO wells. Growth inhibition was then calculated via final cell count divided by initial cell count and presented as a percentage.

Table 4.2 illustrates the descriptive statistics from the 500 nM drug screen, which displays a lower average mean score for BPH-1 (95.9) compared to LnCAP (Parental at 115.9 and MYCN at 101.7). Therefore, BPH-1 showed a lower final cell count compared to LnCAP. But data also showed a negative skew with a high variance BPH-1, LnCAP-P, and LnCAP-MYCN; 1223.6, 1982.1 and 868.2 respectively. The negative skew means that a larger proportion of the data was below the mean, which indicates either many drugs had a significant negative effect on the cells.

Table 4.2 Statistical analysis of 500 nM Targetmol Drug Screen BPH-1 and LnCAP

500 nM	**LNCaP-Parental**	**LNCaP-MYCN**	**BPH-1**
DMSO (# of wells)	107	107	107
Drug Library (# of wells)	1813	1813	1813
Mean Growth Inhibition	115.9072	101.6966	95.8616
Std. Error of Mean	1.01605	0.67245	0.79829
Std. Deviation	44.52127	29.4652	34.97948
Variance	1982.144	868.198	1223.564
Skewness	-0.995	-1.797	-0.911
Std. Error of Skewness	0.056	0.056	0.056
Range	366.52	266.76	224.95
Minimum Growth Inhibition	-95.7	-27.41	-5.16
Maximum Growth Inhibition	270.82	239.35	219.79

From the data, LnCAP-n-MYC was the most sensitive to the drug library at 500 nM, showing the most number of wells below the mean, while BPH-1 and LnCAP-P had similar sensitivity to the

drug library at 500 nM, showing the least number of wells below the mean. Interestingly, MYCN again showed the lowest variance (868.2) compared to the other 2 cell lines, which indicates the difference from the individual wells from the mean was the lowest in the MYCN cell line.

Figure 4.4 illustrates the growth change from the 500 nM drug screen. In LnCAP, results between LnCAP-P and LnCAP-n-MYC were compared. The LnCAP-n-MYC results were below 0 are displayed as LnCAP-n-MYC hits and the LnCAP-P results below 0 are displayed as LnCAP-P hits. Non-LnCAP-P and non-LnCAP-n-MYC hits are values above 0 in both LnCAP-P and LnCAP-n-MYC, and Ln-CAP-P are displayed as Not a hit in LnCAP-P and LnCAP-n-MYC.

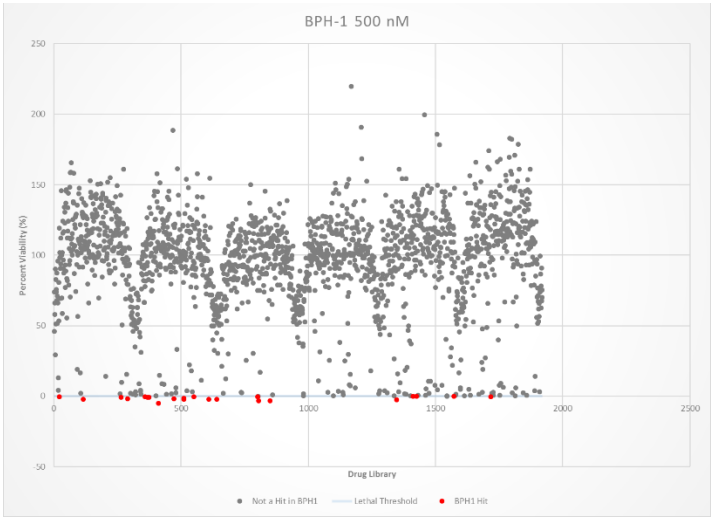

A

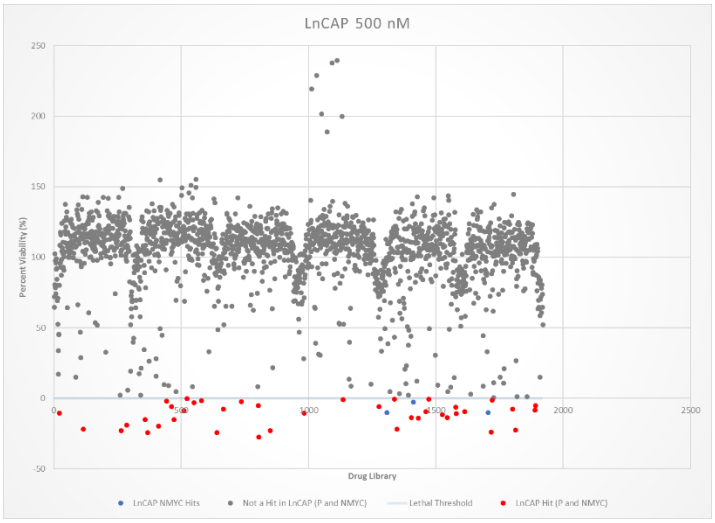

B

Figure 4.4. 500 nM 1813 Drug Screen Distribution. Cell count represent 120 hour post treatment. Cell count was controlled for DMSO. A) 500 nM screen in BPH-1. B) 500 nM screen in LnCAP.

From Figure 4.4, several hits were seen in both BPH-1 and LnCAP at 500 nM. While several hits were seen, a pattern distribution of growth can be seen and reflect the plate distribution. There are 6 waves, which corresponds to the 6 plates involved in the drug screen. Wells located near the edge of the plate show a lower average growth compared to the wells towards the middle of the plate. Therefore, 384-well plate exhibits cell susceptibility with regards to well location at the 500 nM dose concentration like the 100 nM drug screen.

For 1000 nM drug screen, 200 nL of 250 μM of each small molecule was administered to cell lines in a 384-optic plate (#142761). Images were taken at 24, 48, 72, 96 and 120 hours post-treatment, and cell count was adjusted with the average cell count from the 107 DMSO wells. Growth inhibition was then calculated via final cell count divided by initial cell count and presented as a percentage.

Table 4.3 illustrates the descriptive statistics from the 1000 nM drug screen, which displays a lower average mean score for LnCAP-n-MYC (91.7) compared to BPH-1 (100.8) and LnCAP-P (97.9). Therefore, LnCAP-n-MYC showed a lower final cell count compared to BPH-1 and LnCAP-P. But data also showed a negative skew with a high variance BPH-1, LnCAP-P, and LnCAP-MYCN; 1615.1, 1263.1 and 939.2, respectively. The negative skew means that a larger proportion of the data was below the mean, which indicates either many drugs had a significant negative effect on the cells. From the data, LnCAP-n-MYC was the most sensitive to the drug library at 1000 nM, showing the most number of wells below the mean, while BPH-1 and LnCAP-P had similar sensitivity to the drug library at 1000 nM, showing the least number of wells below the mean. Interestingly, MYCN again showed the lowest variance (939.2) compared to the other 2 cell lines, which indicates the difference from the individual wells from the mean was the lowest in the MYCN cell line.

Table 4.3 Statistical analysis of 1000 nM Targetmol Drug Screen BPH-1 and LnCAP

1000 nM	**LNCaP-Parental**	**LNCaP-MYCN**	**BPH-1**
DMSO (# of wells)	107	107	107
Drug Library (# of wells)	1813	1813	1813
Mean Growth Inhibition	97.9265	91.7175	100.8364
Std. Error of Mean	0.8111	0.69939	0.91717
Std. Deviation	35.54049	30.64557	40.18841
Variance	1263.126	939.151	1615.108
Skewness	-0.863	-1.157	-0.798
Std. Error of Skewness	0.056	0.056	0.056
Range	250.71	224.82	244.44
Minimum Growth Inhibition	-24.41	-21.59	-3.34
Maximum Growth Inhibition	226.3	203.23	241.1

Figure 4.5 illustrates the growth change from the 1000 nM drug screen. In LnCAP, results between LnCAP-P and LnCAP-n-MYC were compared. The LnCAP-n-MYC results were below 0 are displayed as LnCAP-n-MYC hits and the LnCAP-P results below 0 are displayed as LnCAP-P hits. Non-LnCAP-P and non-LnCAP-n-MYC hits are values above 0 in both LnCAP-P and LnCAP-n-MYC, and Ln-CAP-P are displayed as Not a hit in LnCAP-P and LnCAP-n-MYC.

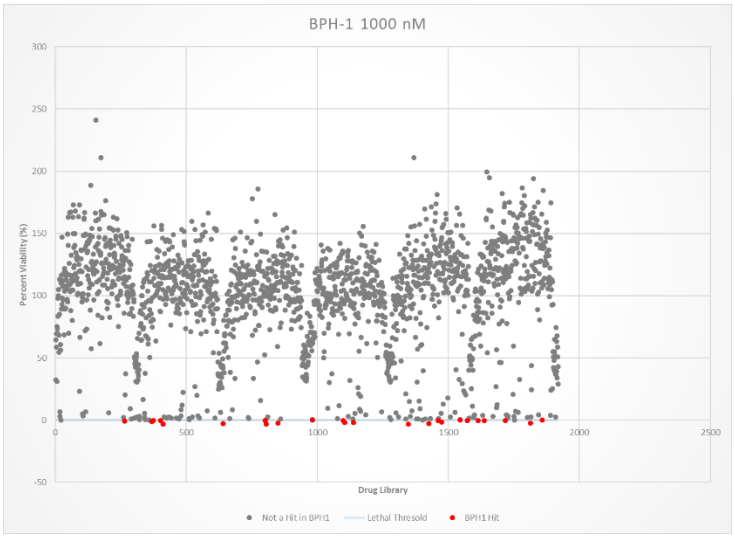

A

Figure 4.5. 1000 nM 1813 Drug Screen Distribution. Cell count represent 120 hour post treatment. Cell count was controlled for DMSO. A) 1000 nM screen in BPH-1. B) 1000 nM screen in LnCAP.

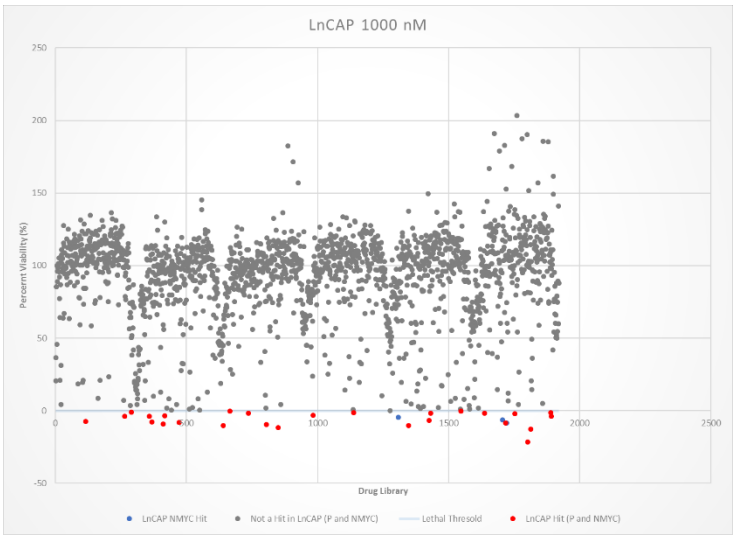

B

From Figure 4.5, several hits were seen in both BPH-1 and LnCAP at 1000 nM. While several hits were seen, a pattern distribution of growth can be seen and reflect the plate distribution. There are 6 waves, which corresponds to the 6 plates involved in the drug screen. Wells located near the edge of the plate show a lower average growth compared to the wells towards the middle of the plate. Therefore, 384-well plate exhibits cell susceptibility with regards to well location at the 1000 nM dose concentration like the 500 nM and 100 nM drug screen.

As result of the common pattern found in all 3 drug screens and among all 3 cell lines, further analysis using variance distribution was used to determine homoscedasticity among data values. Homoscedasticity was determined via SPSS software by comparing standardized residuals of growth inhibition of 3 cells line at 3 concentrations versus the predict values, which is determined by the average response.

Percent Viability Variance Distribution for Targetmol Screen

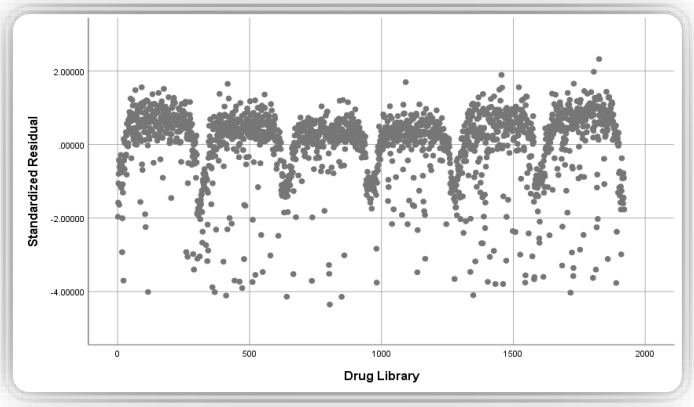

Figure 4.6. Variance Distribution for Targetmol Screen of Percent Viability at 120 hour post treatment for each BPH-1, LnCAP-P, LnCAP-n-MYC at 100 nM, 500 nM, 1000 nM for 2 biological replicates. Residual values from mean average plotted for each drug

Figure 4.6 shows the scatterplot for the standardized residuals for the Targetmol drug library. As can be seen in Figure 4.6, a wave pattern is correlated to plate and well location, irrespective of the cell line or concentration. Therefore, growth inhibition could be attributed to the drug or location of the well. This is a common issue associated with the use of 384-well plates, especially for cultures over 72 hours. A well-documented remedy to this issue is the use of B-score adjustment, which uses the median rather than the mean, since its less susceptible to the skewness of data. Therefore, the B-score analysis was done to control for plate location.

Instead of using mean, a median polish was used to determine B-score for individual wells. This was accomplished by comparing residuals of individual wells and dividing by median absolute deviation. The B-score analysis was done using Python software and a B-score was generated for each cell count for individual well for all 3 cell lines for each of the 3 drug concentrations. Using SPSS software, the standardized residuals were plotted to determine homoscedasticity of B-scores, irrespective of cell line and concentration.

B-score Variance Distribution for Targetmol Screen

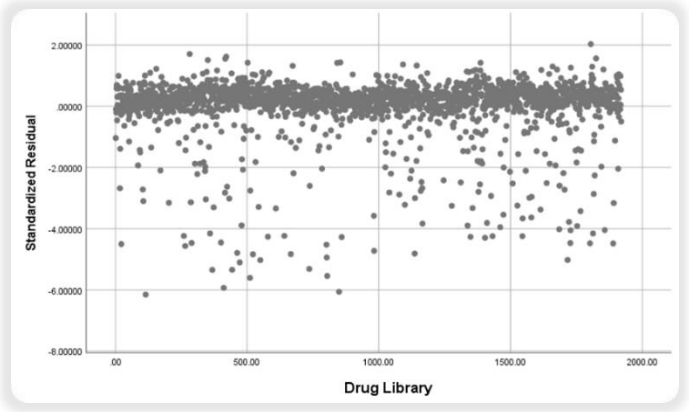

Figure 4.7. Variance Distribution for Targetmol Screen. B-scores represent cell count adjustment of 120 hour post treatment for each BPH-1, LnCAP-P, LnCAP-n-MYC at 100 nM, 500 nM, 1000 nM for 2 biological replicates. Residual values from mean average plotted for each drug.

Figure 4.7 illustrates no discernible pattern among the B-scores, irrespective of the cell line and concentration. Greater than 95% approximate to 0, indicating equal variance among individual wells, except for wells showing considerable growth inhibition, which is irrespective of well or plate location. Therefore, B-score values were determined as valid values to determine growth inhibition for individual drugs in the Targetmol drug library.

To determine the cut-off for the B-score analysis, a distribution curve was assessed to see if data points were normally distributed. All B-scores, from each cell line and all 3 concentrations, were ranked from smallest to largest, and distribution was determined using excel by calculating mean and standard deviation. The frequency analysis was done and data points were plotted.

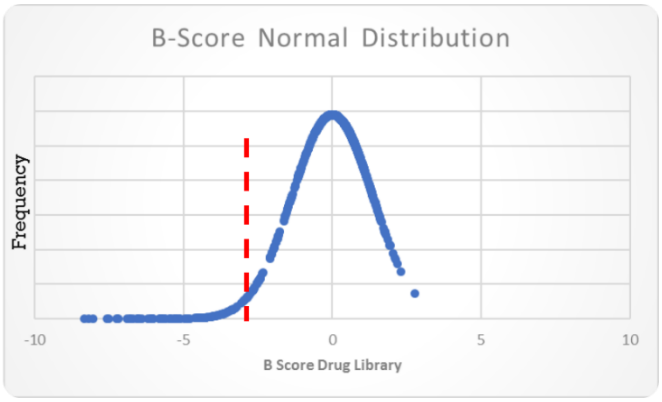

Figure 4.8. Frequency Distribution of B-score. B-scores represent cell count adjustment of 120 hour post treatment for each BPH-1, LnCAP-P, LnCAP-n-MYC at 100 nM, 500 nM, 1000 nM for 2 biological replicates. Normal Distribution Curve.

Figure 4.8 illustrates a normal distribution of B-scores, with a mean of 0 and 2 standard deviation between -3.915 to 3.915, indicating that 95% of all data points fall between -3.915 and 3.915. Points that fell below -3.915 were assessed as probable hits in the screen, as they were significantly different from the average B-score of the drug library. A high B-score illustrates a higher cell count compared to initial concentration, while a lower B-score illustrates a lower cell count compared to initial concentration.

For the 100 nM screen, average B-score was calculated from two individual scores from the 2 biological replicates. Average B-scores for BPH-1 was plotted against the average B-scores for LnCAP (LnCAP-P and LnCAP-n-MYC).

100 nM Targetmol Screen – B-score Adjustment

A

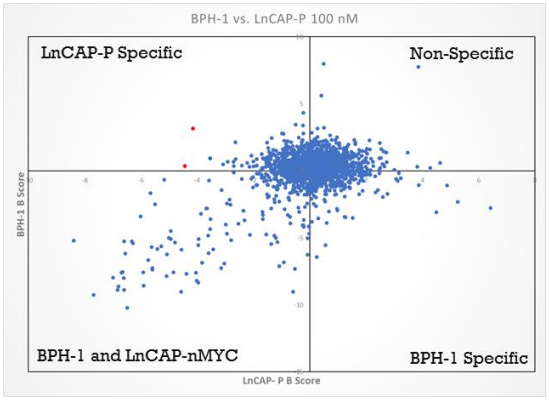

B

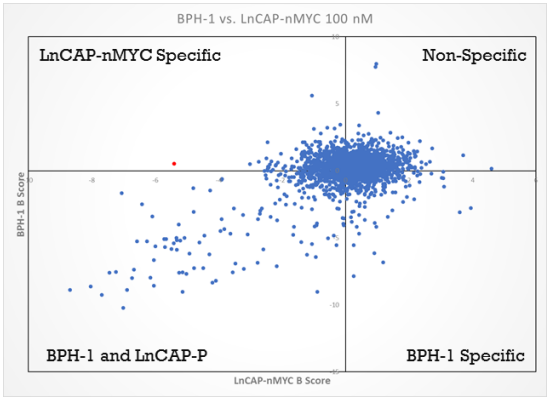

Figure 4.9. BPH-1 B-score vs. LnCAP B-score in 100 nM screen. Cell count represent B-score adjustment of 120 hour post treatment. A) BPH-1 vs. LnCAP-P. B) BPH-1 vs. LnCAP-n-MYC.

Figure 4.9 illustrates BPH-1 vs. LnCAP-P and BPH-1 vs. LnCAP-n-MYC at 100 nM. Top left quadrant represents small molecules that had high B-scores in BPH-1 and low B-scores in LnCAP, which are the compounds of interest for the study. These compounds would have no effect on BPH-1 cell (non-malignant control) while having an inhibitor or negative effect on LnCAP. A cut-off of -3.915 was used to determine if the drug had a significantly negative impact on cell count, and 2 wells were determined as potential LnCAP-P hits and 1 well was determined as a potential LnCAP-n-MYC hit. On plate 3, well A08 had a LnCAP-P B-score of -4.42 and a BPH-1 B-score of 0.36 and the drug dispensed was Pyrilamine Maleate. The second potential

LnCAP-P hit was found on plate 3, in well C08, which had a LnCAP-P B-score -4.13 and BPH-1 B-score of 3.14. The drug found at this location was Hydrocortisone acetate. The potential hit for LnCAP-n-MYC was found on plate 5 at well B10, which had a LnCAP-n-MYC B-score of -5.39 and BPH-1 B-score of 0.53. The drug found at this location was Fludarabine.

Points found in the bottom left quadrant of Figure 4.9 represents drugs that had a negative effect on both BPH-1 and LnCAP, and points found in the bottom right quadrant represent drugs that only had a negative effect on BPH-1. Finally, the top right quadrant were drugs that did not have a negative effect on either BPH-1 or LnCAP. These 3 quadrants were not of interest in this study.

For the 500 nM screen, average B-score was calculated from two individual scores from the 2 biological replicates. Average B-scores for BPH-1 was plotted against the average B-scores for LnCAP (LnCAP-P and LnCAP-n-MYC).

500 nM Targetmol Screen – B-score adjustment

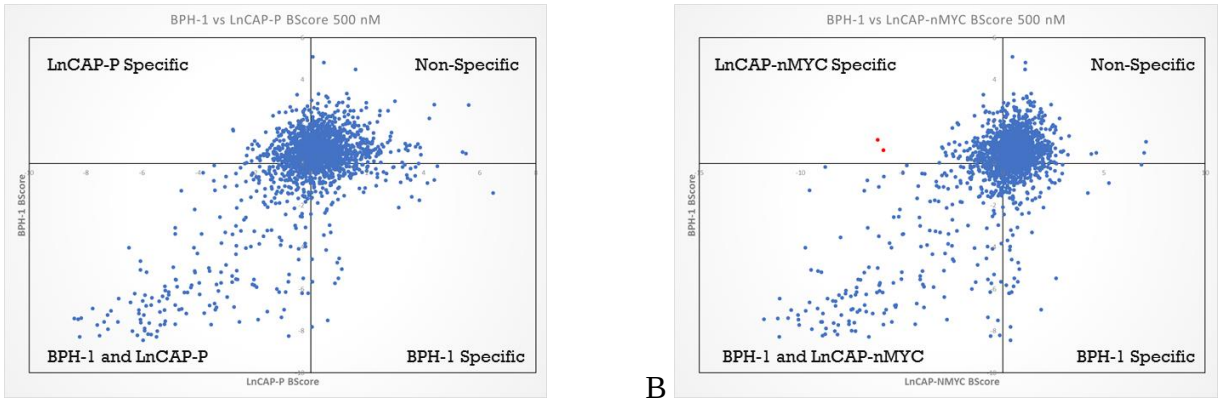

Figure 4.10. BPH-1 B-score vs. LnCAP B-score in 500 nM screen. Cell count represent B-score adjustment of 120 hour post treatment. A) BPH-1 vs. LnCAP-P. B) BPH-1 vs. LnCAP-n-MYC.

Figure 4.10 illustrates BPH-1 vs. LnCAP-P and BPH-1 vs. LnCAP-n-MYC at 500 nM. Top left quadrant represents small molecules that had high B-scores in BPH-1 and low B-scores in LnCAP, which are the compounds of interest for the study. These compounds would have no effect on BPH-1 cell (non-malignant control) while having an inhibitor or negative effect on LnCAP. A cut-off of -3.915 was used to determine if the drug had a significantly negative impact on cell count, and 2 wells were determined as potential LnCAP-P hits and 1 well was determined

as a potential LnCAP-n-MYC hit. There were no LnCAP-P selective drugs found at 500 nM, but 2 LnCAP-n-MYC drugs found.

On plate 2, well E04 had a LnCAP-n-MYC B-score of -5.89 and a BPH-1 B-score of 0.63 and the drug dispensed was Iodoquinol. The second potential LnCAP-n-MYC hit was found on plate 5, in well B10, which had a LnCAP-n-MYC B-score -6.17 and BPH-1 B-score of 1.13. The drug found at this location was Fludarabine, which was also found in the 100 nM Screen.

Points found in the bottom left quadrant of Figure 4.10 represents drugs that had a negative effect on both BPH-1 and LnCAP, and points found in the bottom right quadrant represent drugs that only had a negative effect on BPH-1. Finally, the top right quadrant were drugs that did not have a negative effect on either BPH-1 or LnCAP. These 3 quadrants were not of interest in this study.

For the 1000 nM screen, average B-score was calculated from two individual scores from the 2 biological replicates. Average B-scores for BPH-1 was plotted against the average B-scores for LnCAP (LnCAP-P and LnCAP-n-MYC).

1000 nM Targetmol Screen – B-score adjustment

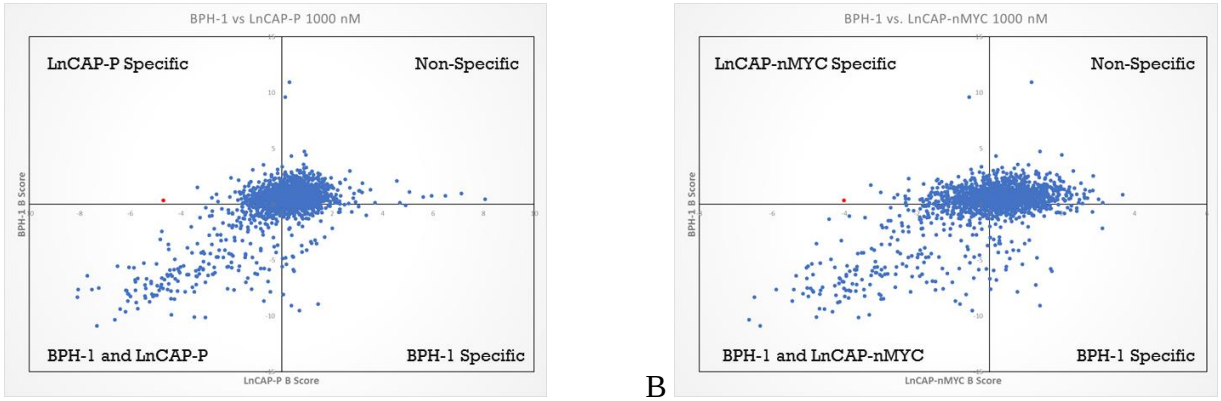

Figure 4.11. BPH-1 B-score vs. LnCAP B-score in 1000 nM screen. Cell count represent B-score adjustment of 120 hour post treatment. A) BPH-1 vs. LnCAP-P. B) BPH-1 vs. LnCAP-n-MYC.

Figure 4.11 illustrates BPH-1 vs. LnCAP-P and BPH-1 vs. LnCAP-n-MYC at 1000 nM. Top left quadrant represents small molecules that had high B-scores in BPH-1 and low B-scores in

LnCAP, which are the compounds of interest for the study. These compounds would have no effect on BPH-1 cell (non-malignant control) while having an inhibitor or negative effect on LnCAP. A cut-off of -3.915 was used to determine if the drug had a significantly negative impact on cell count, and 2 wells were determined as potential LnCAP-P hits and 1 well was determined as a potential LnCAP-n-MYC hit. There were no LnCAP-P selective drugs found at 500 nM, but 2 LnCAP-n-MYC drugs found.

On plate 1, well E08 was found to be a potential hit in both P and MYCN. The LnCAP B-score of -4.67, LnCAP-n-MYC B-score of -4.00 and a BPH-1 B-score of 0.35 and the drug dispensed was Benzethonium chloride.

Points found in the bottom left quadrant Figure 4.11 represents drugs that had a negative effect on both BPH-1 and LnCAP, and points found in the bottom right quadrant represent drugs that only had a negative effect on BPH-1. Finally, the top right quadrant were drugs that did not have a negative effect on either BPH-1 or LnCAP. These 3 quadrants were not of interest in this study.

Fludarabine was selected for further review since it showed MYCN selectivity at the low concentration, as well as the 500 nM. Examination of the average cell counts from the 2 biological replicates and looking at the change over a 5-day course. This is one of the benefits of doing imaging assessment, as day to day changes can be assessed, as compared to an end-point assay. Fludarabine was also found on plate 6 in well F07 as Fludarabine Phosphate, and review of this drug was also included in the review. Fludarabine Phosphate at 100 nM had a BPH-1 B-score of -1.30, LnCAP-P B-score of -1.17 and LnCAP-n-MYC B-score of -4.80. While Fludarabine Phosphate clearly had an inhibitory effect on LnCAP-n-MYC, it also showed an inhibitory effect on BPH-1 and LnCAP-P when compared to the average growth of all the drugs. At 500 nM, Fludarabine Phosphate had a BPH-1 B-score of -1.28, LnCAP-P B-score of -3.41 and LnCAP-n-MYC of -9.55. The cell count was controlled for DMSO, and change was determined by post-treatment cell count divided by pre-treatment cell count and displayed as a percentage.

Table 4.4 100 nM P-value assessment for Fludarabine and Fludarabine Phosphate

Well ID	Small Molecule	Concentration	Cell Line	P-value
5B10	Fludarabine	100 nM	BPH-1	
			LnCAP-P	0.189
			BPH1	
			LnCAP-MYCN	< 0.001
			LnCAP-P	
			LnCAP-MYCN	< 0.001
6F07	Fludarabine Phosphate	100 nM	BPH-1	
			LnCAP-P	0.394
			BPH1	
			LnCAP-MYCN	< 0.001
			LnCAP-P	
			LnCAP-MYCN	< 0.001

Table 4.4 shows that 100 nM of both Fludarabine and Fludarabine Phosphate was statistically different from BPH-1 and LnCAP-P at $\alpha = 0.05$ when comparing 120 hours post treatment cell count change. But the cell count change between BPH-1 and LnCAP-P was not significantly different when using Fludarabine (p-value of 0.189) and Fludarabine Phosphate (p-value of 0.394) at $\alpha = 0.05$. This may indicate MYCN selectivity since both drugs show a significant difference when compared BPH-1(non-malignant control) and LnCAP-P (malignant control).

100 nM Targetmol Screen for Fludarabine and Fludarabine Phosphate

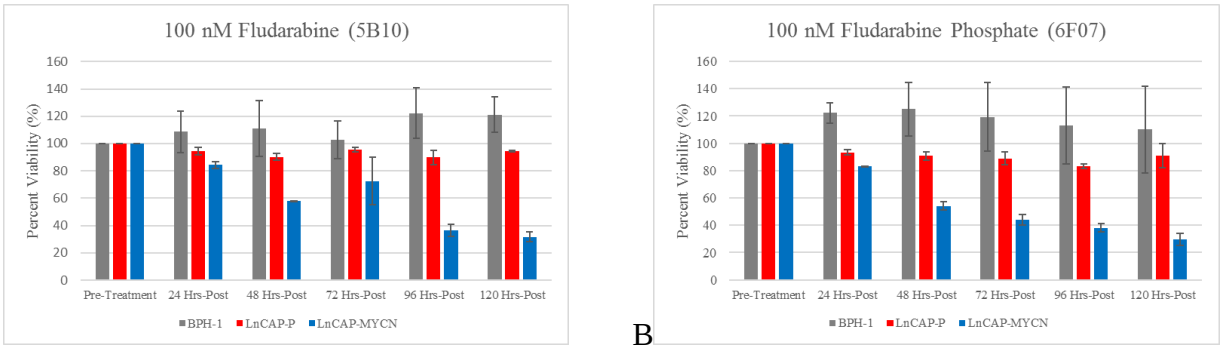

A B

Figure 4.12. Percent Viability at 100 nM. Cells were seeded and Pre-treatment count was determined 24 hours after seeding. Drug library was dispensed after Pre-treatment images were taken. Cell count was controlled for DMSO. A) Fludarabine B) Fludarabine Phosphate

Figure 4.12 illustrates the change in cell count from 24 hours post-treatment to 120 hours post-treatment for both Fludarabine and Fludarabine Phosphate at 100 nM. Both drugs began to show a noticeable difference in cell count change after 48 hours post-treatment when compared to both BPH-1 and LnCAP-P. On average, BPH-1 cell count change increased when compared to pre-

treatment, while LnCAP-P showed a slight decrease in cell count change. Fludarabine Phosphate had a consistent trend downward in the LnCAP-n-MYC when compared to Fludarabine, as at 72-hours post-treatment, there was a rise in cell count change. Interestingly, Fludarabine phosphate did not show up when looking at B-score change due to the negative effect it had on BPH-1. This is probably due to the high variability in the cell count scores in BPH-1, which is illustrated by the large error bar. In Fludarabine, error bars are smaller and present higher than pre-treatment cell count.

Table 4.5 500 nM P-value assessment for Fludarabine and Fludarabine Phosphate

Well ID	Small Molecule	Concentration	Cell Line	P-value
5B10	Fludarabine	500 nM	BPH-1	
			LnCAP-P	0.775
			BPH1	
			LnCAP-MYCN	< 0.001
			LnCAP-P	
			LnCAP-MYCN	< 0.001
6F07	Fludarabine Phosphate	500 nM	BPH-1	
			LnCAP-P	0.392
			BPH1	
			LnCAP-MYCN	< 0.001
			LnCAP-P	
			LnCAP-MYCN	< 0.001

Table 4.5 show that 500 nM of both Fludarabine and Fludarabine Phosphate was statistically different from BPH-1 and LnCAP-P at $\alpha = 0.05$ when comparing 120 hours post treatment cell count change. But the cell count change between BPH-1 and LnCAP-P was not significantly different when using Fludarabine (p-value of 0.775) and Fludarabine Phosphate (p-value of 0.392) at $\alpha = 0.05$. This also indicates MYCN selectivity, but also similar effects on BPH-1 and LnCAP-P at 100 nM.

500 nM Targetmol Screen for Fludarabine and Fludarabine Phosphate

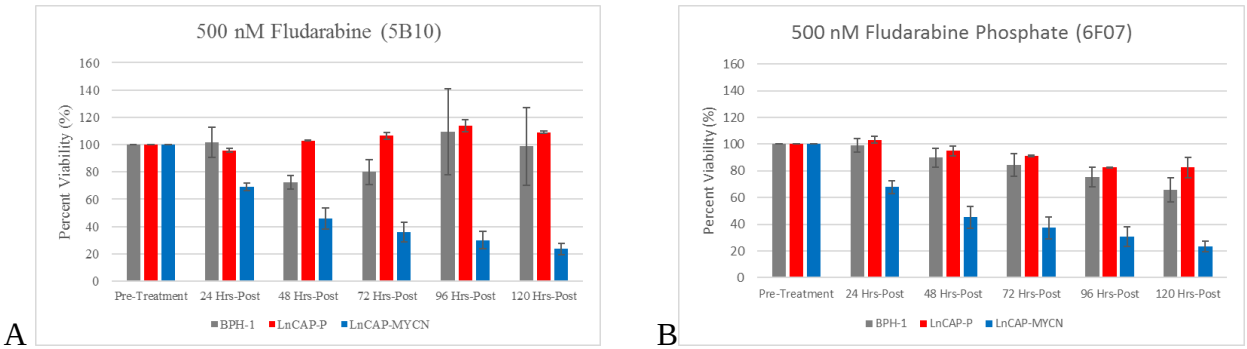

Figure 4.13. Percent Viability at 500 nM. Cells were seeded and Pre-treatment count was determined 24 hours after seeding. Drug library was dispensed after Pre-treatment images were taken. Cell count was controlled for DMSO. A) Fludarabine B) Fludarabine Phosphate

Figure 4.13 illustrates the change in cell count from 24-hours post-treatment to 120-hours post-treatment for both Fludarabine and Fludarabine Phosphate at 500 nM. Both drugs began to show a noticeable difference, but changes are similar in the LnCAP-n-MYC from 24-hours post-treatment to 120-hours post-treatment. The key difference between Fludarabine and Fludarabine Phosphate was in BPH-1 and LnCAP-P. Fludarabine Phosphate seems to have a similar inhibitory effect on BPH-1 and LnCAP-P, while Fludarabine seems to have an inhibitory effect on BPH-1 after 48 hours post-treatment, which rebounded after 96 hours post-treatment. Fludarabine doesn't seem to have the same inhibitory effect on LnCAP-P as Fludarabine Phosphate. Due to Fludarabine Phosphate inhibitory effect on BPH-1, its congruent with B-score analysis, which showed a negative impact on BPH-1.

Table 4.6 1000 nM P-value assessment for Fludarabine and Fludarabine Phosphate

Well ID	Small Molecule	Concentration	Cell Line	P-value
5B10	Fludarabine	1000 nM	BPH-1	
			LnCAP-P	0.100
			BPH1	
			LnCAP-MYCN	< 0.001
			LnCAP-P	
			LnCAP-MYCN	< 0.001
6F07	Fludarabine Phosphate	1000 nM	BPH-1	
			LnCAP-P	0.308
			BPH1	
			LnCAP-MYCN	< 0.001
			LnCAP-P	
			LnCAP-MYCN	< 0.001

Table 4.6 show that 1000 nM of both Fludarabine and Fludarabine Phosphate was statistically different from BPH-1 and LnCAP-P at $\alpha = 0.05$ when comparing 120 hours post treatment cell count change. But the cell count change between BPH-1 and LnCAP-P was not significantly different when using Fludarabine (p-value of 0.100) and Fludarabine Phosphate (p-value of 0.308) at $\alpha = 0.05$. Interestingly, while both show MYCN selectivity, Fludarabine Phosphate p-value is similar between BPH-1 and LnCAP-P as seen at 100 nM and 500 nM.

1000 nM Targetmol Screen for Fludarabine and Fludarabine Phosphate

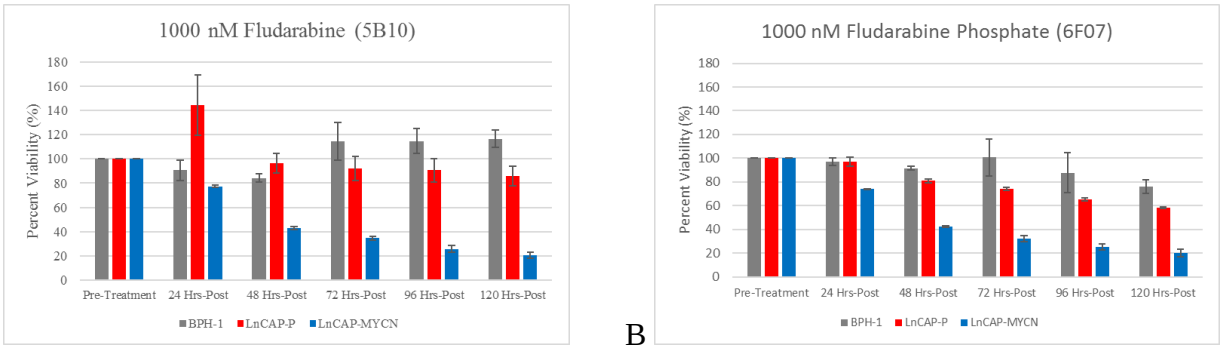

Figure 4.14. Percent Viability at 1000 nM. Cells were seeded and Pre-treatment count was determined 24 hours after seeding. Drug library was dispensed after Pre-treatment images were taken. Cell count was controlled for DMSO. A) Fludarabine B) Fludarabine Phosphate

Figure 4.14 illustrates the change in cell count from 24 hours post-treatment to 120 hours post-treatment for both Fludarabine and Fludarabine Phosphate at 1000 nM. Again, both drugs showed similar inhibition patterns in LnCAP-n-MYC, with noticeable differences taking place 48 hours post-treatment. Fludarabine Phosphate also showed more inhibition in BPH-1 and LnCAP-P compared to Fludarabine, which was seen at 500 nM. But unlike at 500 nM, Fludarabine shows inhibition in LnCAP-P, which wasn't seen in the 500 nM screen. Due to Fludarabine Phosphate inhibitory effect on BPH-1, its congruent with B-score analysis, which showed a negative impact on BPH-1.

After looking at cell count change and B-score, Fludarabine and Fludarabine Phosphate seem like potential MYCN selective drug that may selectively in LnCAP-n-MYC in NEPC. Since Fludarabine Phosphate is currently clinical being used, due to its oral route and increased

bioavailability, it has the greatest potential for drug repurposing and therefore further evaluation will be done in Fludarabine Phosphate.

4.3 Validation and Dose-Response Curve of Fludarabine Phosphate

To validate LnCAP-MYCN sensitivity to Fludarabine Phosphate, Alamar Blue Cell Viability test was done. In addition, the 22rv1 (Parental and nMYC overexpressed) cell lines were added, as they have also been shown in NEPC models. Therefore, the 5 cell lines used in the validation were BPH-1, LnCAP-P, LnCAP-n-MYC, 22rv1-P, and 22rv1-n-MYC.

Table 4.7 Validation of Fludarabine Phosphate

	Percent Viability (%)									
	BPH-1	**BPH-1 S.D**	**LnCAP-P**	**LnCAP-P S.D**	**LnCAP-MYCN**	**LnCAP-MYCN S.D**	**22rv1-P**	**22rv1-P S.D**	**22rv1-MYCN**	**22rv1-MYCN S.D**
12800 nM	65.303	3.547	47.483	3.078	30.568	1.631	53.424	3.952	50.802	8.018
6400 nM	85.618	2.741	59.103	4.597	30.687	1.554	62.797	11.486	56.876	9.328
3200 nM	92.875	1.389	60.945	3.504	34.919	2.369	63.492	10.372	63.700	10.753
1600 nM	94.956	1.220	72.529	10.327	33.142	0.946	69.804	8.174	61.003	8.362
800 nM	92.679	3.233	73.867	12.756	32.813	2.107	82.315	4.821	56.154	2.089
400 nM	96.816	1.074	89.342	3.372	41.829	5.634	87.403	6.924	61.553	5.176
200 nM	97.253	1.012	95.767	5.051	58.759	12.329	91.521	6.391	63.439	4.658
100 nM	97.461	2.530	98.284	0.404	68.837	11.520	88.763	6.461	75.694	10.087
50 nM	98.288	1.159	96.637	2.187	78.796	10.862	100.017	7.848	82.687	8.171
25 nM	99.034	0.798	84.840	17.561	67.112	7.341	100.862	10.497	86.870	11.669
DMSO	100.000	0.000	100.000	0.000	100.000	0.000	100.000	0.000	100.000	0.000

Table 4.7 and Figure 4.15 illustrates the effectiveness of Fludarabine phosphate, not only in n-MYC overexpressed cell lines, but all NEPC cell lines compared to BPH-1. Percent viability was remained above 50% even at the highest concentration (12800 nM), while the percent viability for LnCAP-P, 22rv1-P and 22rv1-nMYC dropped to approximately 50% at 12800 nM. LnCAP-nMYC fell below 50% between 200 nM and 400 nM.

A

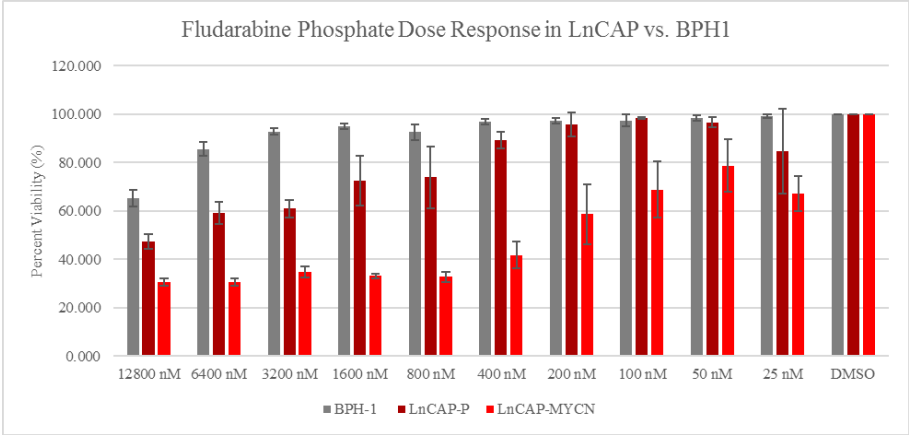

B

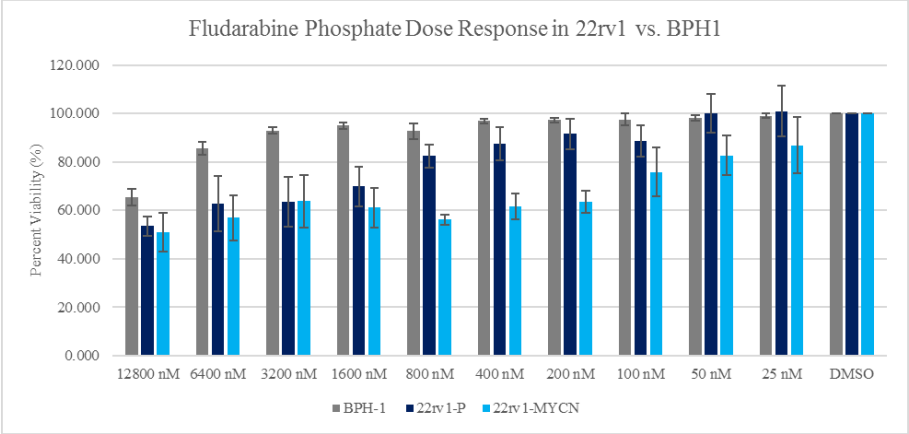

Figure 4.15. Percent Viability between 12800 nM to 25 nM of Fludarabine Phosphate. Cell count was determined at pre-treatment, 96 hours post-treatment and 120 hours post-treatment. Cell count was controlled for DMSO. A) BPH-1 vs. LnCAP B) BPH-1 vs. 22rv1

Table 4.8 illustrates p-values associated with Fludarabine-phosphate validation. BPH-1 percent viability was significantly different from LnCAP-P at concentrations 3200 nM to 6400 nM, while significantly different from LnCAP-nMYC at concentrations greater than 100 nM. In comparison to 22rv1, BPH-1 was significantly different from 22rv1-P at 3200 nM, while significantly different from 22rv1-nMYC between 200 nM to 6400 nM. Comparing isometric pairs (LnCAP-P vs. LnCAP-nMYC and 22rv1-P vs. 22rv1-nMYC), LnCAP cell lines were significantly different at concentrations between 100 nM to 6400 nM, while 22rv1 cell lines were significantly different at concentrations between 200 nM to 800 nM.

Table 4.8 Fludarabine Phosphate Validation p-values in BPH-1, LnCAP and 22rv1

	BPH-1 vs. LnCAP-P p-value	BPH-1 vs. LnCAP-nMYC p-value	BPH-1 vs. 22rv1-P p-value	BPH-1 vs. 22rv1-nMYC p-value
12800 nM	0.093	< 0.001	0.348	0.178
6400 nM	0.028	< 0.001	0.061	0.016
3200 nM	0.010	< 0.001	0.019	0.020
1600 nM	0.083	< 0.001	0.050	0.007
800 nM	0.145	< 0.001	0.433	0.003
400 nM	0.584	< 0.001	0.488	0.005
200 nM	0.915	0.002	0.677	0.008
100 nM	0.953	0.026	0.524	0.098
50 nM	0.906	0.143	0.902	0.246
25 nM	0.295	0.013	0.897	0.372

	LnCAP-P vs. LnCAP-nMYC p-value	22rv1-P vs. 22rv1-nMYC p-value
12800 nM	0.056	0.683
6400 nM	0.003	0.588
3200 nM	0.008	0.985
1600 nM	< 0.001	0.442
800 nM	< 0.001	0.026
400 nM	< 0.001	0.034
200 nM	0.003	0.024
100 nM	0.023	0.308
50 nM	0.178	0.200
25 nM	0.150	0.191

Figure 4.16 and Table 4.9 illustrates the dose-response curve with IC50 values at 120 hours post-treatment with Fludarabine Phosphate in BPH-1, LnCAP-P, LnCAP-n-MYC, 22rv1-P, and 22rv1-n-MYC. MYCN overexpressing cell lines showed a higher sensitivity to Fludarabine Phosphate, presenting with lower IC50 values compared to their isogenic pair.

Table 4.9 Fludarabine Phosphate IC50

	IC50 Value	95% C.I
BPH-1	23280 nM	15831 to 34236
LnCAP-P	9947 nM	5423 to 18244
LnCAP-MYCN	426.5 nM	215.7 to 843.1
22rv1-P	13854 nM	8338 to 23018
22rv1-MYCN	9923 nM	2469 to 39873

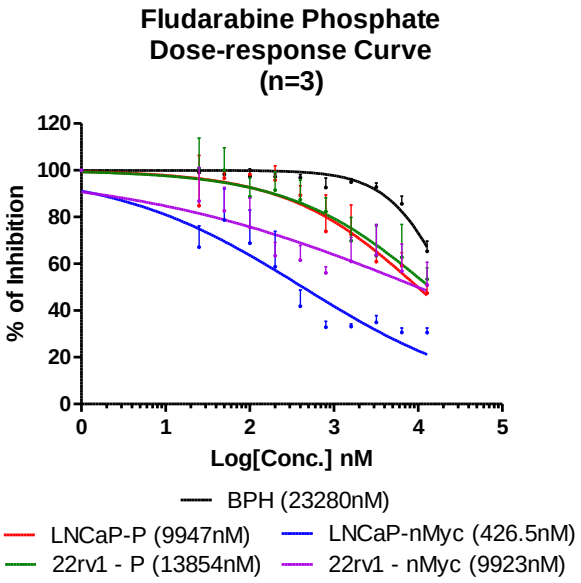

Figure 4.16. Dose-Response Curve for Fludarabine Phosphate. Cell count was controlled for DMSO.

LnCAP-P and 22rv1-P showed comparable sensitivities, with IC50 values of 9947 nM and 13854 nM, respectively. But LnCAP-n-MYC showed a higher sensitivity than 22rv1-n-MYC, with IC50 values of 426.5 nM and 9923 nM. The similarity between LnCAP-P and 22rv1-nMYC may be due to the subtle expression of MYCN in LnCAP-P. Ultimately, both LnCAP and 22rv1 show increased sensitivity compared to BPH-1, the non-malignant control, which had an approximate IC50 value of 23280 nM.

5. Discussion of Results

Fludarabine phosphate, which is marketed as Fludara, is a prodrug of Fludarabine, which is a fluorinated nucleotide antimetabolite analog of vidarabine that displays antineoplastic activity. But unlike vidarabine, adenosine deaminase does not deaminate fludarabine phosphate. Fludarabine acts as nucleoside metabolic inhibitors, which inhibit nucleic acid synthesis.[95]

Fludarabine was initially developed as an antineoplastic agent used for hematological malignancies, specifically chronic lymphocytic leukemia and B-cell lymphomas, but has also been used in the treatment of a variety of other cancers and conditions for its immunosuppressive properties.[96]

Pharmacokinetic studies have shown similar exposure between oral dose versus intravenous dose, but adjustments need to be made in patients with renal impairment. The National Institute for Clinical Excellence (NICE) recommended in 2001 that oral Fludarabine phosphate is used instead of the intravenous version, and subsequently, it was approved by the US Food and Drug for treatment of CLL in 2008. [95]

Fludarabine a pyrimidine and purine analog (PA), which belongs to the family of nucleoside analogs (NA). These antimetabolites were initially used to treat hematologic cancers, but are now being used for solid tumors as well. First generation PA’s include 6-mercaptopurine and 6-

thioguanine, which were used in the treatment of acute leukemias, while second-generation PA's consist of cladribine, pentostatin, and fludarabine.[95]

5.1 Fludarabine Pharmacodynamics

Fludarabine phosphate is the phosphate salt of Fludarabine that is rapidly dephosphorylated by nucleotidase activity to fluoro-ara-A, which is taken up by cells. Inside the cell, fluoro-ara-A is dephosphorylated to monophosphate, diphosphate, and triphosphate by deoxycytidine kinase, whereby fluoro-ara-ATP appears to be the only metabolite with cytotoxic properties causing inhibition of DNA and RNA synthesis by inhibiting DNA polymerases, DNA primase, DNA ligase, and ribonucleotide reductase, as well as partial inhibition of RNA polymerase II.[97] This cytotoxic effect primarily takes place in S-phase of cell division. Fluoro-ara-AMP leads to gene transcription repression, which ultimately leads to decreased expression of proteins involved in cell survival and causing apoptosis.[98]

5.2 Fludarabine Pharmacokinetics

The bioavailability between oral and intravenous formulation is similar in Fludarabine phosphate; 50-75% in oral versus 75% intravenous formulation. However, the maximum plasma concentration (C_{max}) was similar between oral and intravenous formulation when measured between 30 to 60 minutes after infusion, as well as proportional changes in plasma concentration-time curves (AUC) with increased IV dosages compared to similar oral dosages.[95, 99, 100] Fludarabine has a volume distribution of 83-98 L/m2, but is does not cross the blood brain barrier or bind to plasma proteins.[101]

The half-life for Fluoro-ara-A can range from hours to days and is eliminated by renal excretion, with approximately 37% occurs within the first 24 hours and more than half within 72 hours after administration, in both intravenous and oral administration.[95] Special attention should be given to patients with impaired renal function and therefore dosage should reflect renal function. As a result, oral formulation ($40mg/m^2/d$) immediate-release tablets were given preference over IV formulation ($25/m^2/d$) in 2001 by the NICE. The oral formulation not only had similar

pharmacokinetics, but there was no need for repetitive puncture wounds or need for catheters, as well as the IV-related complications, such as thrombosis, bleeding, and infection. Another important benefit was the reduced medical costs for patients, as it required fewer hospital visits and related costs. [95, 102]

5.3 Fludarabine Adverse Effects

The most common adverse effects occur due to the bone marrow suppression, which is also the major dose-limiting side-effect. Adverse effects in all 3 bone marrow cell lines are seen in patients taking Fludarabine; neutropenia (low neutrophil count), thrombocytopenia (low platelet count) and anemia (low red blood cell count) occur in 38%, 15%, and 18% respectively.[103] Prolonged cytopenia can occur and may take several months to resolve even after fludarabine phosphate has been discontinued.[95] Due to the immunosuppressive effects, fludarabine phosphate only increases the risk of bacterial infections, but also opportunistic infections, such as Listeria, Nocardia, Candida, as well as others. As a result, some clinicians recommend antibacterial and antiviral prophylaxis during treatment.[104]

Neurotoxicity is seen with high doses of fludarabine (>96 $mg/m^2/d$), which consist of altered mental status, seizures, paraparesis, encephalopathy, ocular toxicity and even comas.[105] But while neurotoxicity is typically rare, progressive multifocal leukoencephalopathy (PML) must be ruled out once neurologic symptoms present. PML is the diffuse and progressive inflammation of the white matter of the brain, which is typically fatal. Treatment of fludarabine-induced neurotoxicity is discontinuing treatment immediately.[95] Gastrointestinal symptom, such as nausea, vomiting, and diarrhea, occur in less than 5% of cases, and while this isn't a major adverse effect, it is particularly important when prescribing oral formulation. Therefore, IV formulation should be considered for any patient that displays gastrointestinal symptoms.[96]

Another rare complication of fludarabine treatment is tumor lysis syndrome (TLS), which a metabolic disorder that occurs from chemotherapy treatment. Due to high tumor cell death, large amounts of intracellular contents are released into the bloodstream and results in elevated uric acid, potassium, and phosphorus, as well as a decrease calcium level. It is recommended that

patients have adequate oral hydration as well as allopurinol prophylaxis to prevent TLS.[106] Fludarabine phosphate is frequently combined with corticosteroids, which can precipitate infection severity and incidence.[95]

5.4 Drug Interactions

Drug-drug interactions have been shown to occur with other anti-neoplastic and immunosuppressive agents.[100] Adverse effects have been shown when fludarabine phosphate is combined with cabazitaxel and clozapine.[100, 107] Cabazitaxel is a microtubule inhibition that is currently indicated metastatic prostate cancer previously treated with docetaxel. Clozapine is an atypical antipsychotic that inhibits both serotonin and dopamine, which may be used in patients with previous psychiatric conditions or onset of neurologic symptoms associated with fludarabine phosphate.[108] Significant interactions between Fludarabine and cytarabine, another chemotherapy agents used in the treatment of leukemia. Cytarabine decreases fludarabine metabolism by competing with deoxycytidine kinase. Fludarabine also interacts with pentostatin, another chemotherapy agent that is a nucleic acid synthesis inhibitor. The mechanism of action for the interaction is unknown, but the combination leads to fatal pneumonitis.[97, 109]

5.5 Fludarabine Clinical Applications

The primary use for Fludarabine phosphate is in the treatment of Leukemia, specifically chronic lymphocytic leukemia and prolymphocytic leukemia, as well as non-Hodgkin's lymphoma. But it has also been shown to be effective in treating acute myeloid leukemia, hairy cell leukemia, cutaneous T-cell lymphoma, and Waldenstrom's macroglobulinemia, as well as a regimen for pre-allogenic bone marrow transplant.[101, 109] Fludarabine phosphate is classified as a Category D, as there is evidence of for fetal risk, but benefits may be acceptable despite the risk.[110]

5.6 Future Direction

The transition from *in vitro* studies to clinical use is a major challenge for repurposed small molecules found in high-throughput screens. Therefore, the next step involves a 2-step process; *in vivo* studies involving Fludarabine and/or Fludarabine Phosphate and knockdown studies involving gene targets associated with Fludarabine. First, *in vivo* studies that involve animal models with NEPC tumors that express n-MYC versus NEPC tumors that do not express n-MYC can give valuable data about Fludarabine and/or Fludarabine Phosphate ability to cause tumor regression in a biological system. Tumor size as well as immunohistochemistry for NEPC markers, such as chromogranin (CgA), synaptophysin (SYP) and neuron-specific enolase (NSE), can give insight on the effectiveness of Fludarabine and/or Fludarabine Phosphate in the treatment of NEPC. Second, Fludarabine is associated with p53 genes associated with DNA repair, which include *PCNA, RRM2B, TP53AP1, XPC, CHD2, DDB2, HDAC9, MLH1* and *MSH6*.[111, 112] Knockdown studies involving these genes, as well as genes associated with DNA polymerases, DNA primase, DNA ligase, ribonucleotide reductase, and RNA polymerase II, may yield mechanism knowledge of Fludarabine selectivity for n-MYC positive NEPC cells.

6. Conclusion

There is a pressing need for continued research in rare conditions, as these conditions are often overlooked due costs involved in discovering therapeutic agents, which include the costs for development and clinical assessment. High-throughput screens for therapeutic repurposing can be a viable option for these conditions, as the there are no initial costs associated with these studies as FDA approved drugs have already gone through clinical trials. High-throughput screens can also be effective in drug-resistant conditions, whereby the mechanism of action for resistance is unknown. Since a great deal of knowledge is known about FDA approved drugs, hits that show up on high-throughput screens for drug-resistant conditions may provide insight on mechanism, while also provide potential therapeutic agents ready for clinical use.

Cancer treatment has moved away from one-size-fits-all approach to personalized therapy involving molecular alterations in tumors. This allows for multi-organ treatment that occurs with metastasis, without targeting health tissue that doesn't express molecular marker. The difficulty arises in finding unique molecular targets that are not expressed in non-cancer tissue, as well as finding small molecules that target these molecular alterations.

Neuroendocrine prostate cancer (NEPC) is condition that arises from androgen deprivation of prostate adenocarcinoma. While this condition only affects about 2,000 Canadian males per year, it results in death within a year of diagnosis approximately 98% of the time. With the expected rise in incidence for prostate cancer and the use of stronger antiandrogens, the rise of NEPC is expected to rise, and unfortunately, there is no treatment to date. NEPC has been shown to overexpress MYCN, which is a known proto-oncogene that is not typically expressed in adult tissue. MYCN is associated with tumors arising from the neural system, and commonly expressed in all forms of Neuroendocrine cancers.

The high-throughput screen of the Targetmol Drug Library detected a potential therapeutic agent for NEPC cells that overexpress MYCN. Flurdarabine and Fludarabine phosphate (Fludarabine prodrug) showed selectivity in NEPC cells (LnCAP and 22rv1) that overexpressed MYCN, but also showed potency in cancer cells compared to non-cancer cells (BPH-1). This maybe due to Fludarabine ability to inhibit RNA polymerase II or ribonucleotide reductase, as MYCN is associated with both. But further research involving knockdown genes may yield understanding of Fludarabine and Fludarabine phosphate mechanism for MYCN selectivity is needed.

The results from the high-throughput imaging screen of the Targetmol Drug library have led to a promising candidate for the treatment of n-MYC positive NEPC cells. While this study only revealed a small part of the NEPC puzzle, it has open the door for potential research for in vivo studies involving Fludarabine and/or Fludarabine phosphate for n-MYC positive cancer cells, as well as knockdown studies involving genes associated with Fludarabine. But the key benefit of this screen was that it yielded a potential therapeutic agent that can benefit patients immediately, since Fludarabine phosphate is FDA approved for patients with hematological cancers.

References

1. Beltran, H., et al., *Challenges in recognizing treatment-related neuroendocrine prostate cancer.* J Clin Oncol, 2012. **30**(36): p. e386-9.
2. Gregory, C.W., et al., *Androgen receptor expression in androgen-independent prostate cancer is associated with increased expression of androgen-regulated genes.* Cancer Res, 1998. **58**(24): p. 5718-24.
3. Hellerstedt, B.A. and K.J. Pienta, *The current state of hormonal therapy for prostate cancer.* CA Cancer J Clin, 2002. **52**(3): p. 154-79.
4. Cancer, C.C.S.s.A.C.o. and Statistics., *Canadian Cancer Statistics 2017.* 2017.
5. Center, M.M., et al., *International variation in prostate cancer incidence and mortality rates.* Eur Urol, 2012. **61**(6): p. 1079-92.
6. Ilic, D., et al., *Screening for prostate cancer.* Cochrane Database Syst Rev, 2013(1): p. CD004720.
7. Etzioni, R., et al., *Overdiagnosis due to prostate-specific antigen screening: lessons from U.S. prostate cancer incidence trends.* J Natl Cancer Inst, 2002. **94**(13): p. 981-90.
8. Vickers, A.J., et al., *Empirical estimates of prostate cancer overdiagnosis by age and prostate-specific antigen.* BMC Med, 2014. **12**: p. 26.
9. Loeb, S., et al., *Overdiagnosis and overtreatment of prostate cancer.* Eur Urol, 2014. **65**(6): p. 1046-55.
10. Fitzpatrick, J.M., E. Banu, and S. Oudard, *Prostate-specific antigen kinetics in localized and advanced prostate cancer.* BJU Int, 2009. **103**(5): p. 578-87.
11. Loeb, S., *Guideline of guidelines: prostate cancer screening.* BJU Int, 2014. **114**(3): p. 323-5.
12. National Cancer Institute Surveillance, E.a.E.R.P., *Prostate Cancer.* 2017.
13. Brawley, O.W., *Trends in prostate cancer in the United States.* J Natl Cancer Inst Monogr, 2012. **2012**(45): p. 152-6.
14. Bostwick, D.G., et al., *Human prostate cancer risk factors.* Cancer, 2004. **101**(10 Suppl): p. 2371-490.
15. Deloumeaux, J., et al., *Prostate cancer clinical presentation, incidence, mortality and survival in Guadeloupe over the period 2008-2013 from a population-based cancer registry.* Cancer Causes Control, 2017. **28**(11): p. 1265-1273.
16. McKenney, J.K., *The present and future of prostate cancer histopathology.* Curr Opin Urol, 2017. **27**(5): p. 464-468.
17. Epstein, J.I., et al., *The 2014 International Society of Urological Pathology (ISUP) Consensus Conference on Gleason Grading of Prostatic Carcinoma: Definition of Grading Patterns and Proposal for a New Grading System.* Am J Surg Pathol, 2016. **40**(2): p. 244-52.
18. Beltran, H., et al., *Molecular characterization of neuroendocrine prostate cancer and identification of new drug targets.* Cancer Discov, 2011. **1**(6): p. 487-95.
19. Tagawa, S.T., *Neuroendocrine prostate cancer after hormonal therapy: knowing is half the battle.* J Clin Oncol, 2014. **32**(30): p. 3360-4.
20. Klotz, L., *Combined androgen blockade: an update.* Urol Clin North Am, 2006. **33**(2): p. 161-6, v-vi.
21. Huggins, C. and C.V. Hodges, *Studies on prostatic cancer. I. The effect of castration, of estrogen and androgen injection on serum phosphatases in metastatic carcinoma of the prostate.* CA Cancer J Clin, 1972. **22**(4): p. 232-40.
22. Labrie, F., et al., *Combination therapy for prostate cancer. Endocrine and biologic basis of its choice as new standard first-line therapy.* Cancer, 1993. **71**(3 Suppl): p. 1059-67.

23. Auchus, R.J. and W.E. Rainey, *Adrenarche - physiology, biochemistry and human disease.* Clin Endocrinol (Oxf), 2004. **60**(3): p. 288-96.
24. Wierman, M.E., et al., *Adrenarche and skeletal maturation during luteinizing hormone releasing hormone analogue suppression of gonadarche.* J Clin Invest, 1986. **77**(1): p. 121-6.
25. Knorr, D., et al., *Plasma testosterone in male puberty. I. Physiology of plasma testosterone.* Acta Endocrinol (Copenh), 1974. **75**(1): p. 181-94.
26. Stocco, D.M., *The steroidogenic acute regulatory (StAR) protein.* Medicina (B Aires), 1999. **59**(5 Pt 2): p. 538-9.
27. Labrie, F., et al., *New hormonal therapy in prostatic carcinoma: combined treatment with an LHRH agonist and an antiandrogen.* Clin Invest Med, 1982. **5**(4): p. 267-75.
28. McLeod, D.G., *Tolerability of Nonsteroidal Antiandrogens in the Treatment of Advanced Prostate Cancer.* Oncologist, 1997. **2**(1): p. 18-27.
29. Polotti, C.F., et al., *Androgen deprivation therapy for the treatment of prostate cancer: a focus on pharmacokinetics.* Expert Opin Drug Metab Toxicol, 2017. **13**(12): p. 1265-1273.
30. Singer, E.A., et al., *Androgen deprivation therapy for prostate cancer.* Expert Opin Pharmacother, 2008. **9**(2): p. 211-28.
31. Ortmann, O., J.M. Weiss, and K. Diedrich, *Gonadotrophin-releasing hormone (GnRH) and GnRH agonists: mechanisms of action.* Reprod Biomed Online, 2002. **5 Suppl 1**: p. 1-7.
32. Mahler, C., J. Verhelst, and L. Denis, *Clinical pharmacokinetics of the antiandrogens and their efficacy in prostate cancer.* Clin Pharmacokinet, 1998. **34**(5): p. 405-17.
33. Gao, W., J. Kim, and J.T. Dalton, *Pharmacokinetics and pharmacodynamics of nonsteroidal androgen receptor ligands.* Pharm Res, 2006. **23**(8): p. 1641-58.
34. Thakur, A., et al., *Abiraterone acetate in the treatment of prostate cancer.* Biomed Pharmacother, 2018. **101**: p. 211-218.
35. Roehrborn, C.G. and L.K. Black, *The economic burden of prostate cancer.* BJU Int, 2011. **108**(6): p. 806-13.
36. Canada, P.H.A.o., *Economic Burden of Illness in Canada.* 2011.
37. Yamaoka, M., T. Hara, and M. Kusaka, *Overcoming persistent dependency on androgen signaling after progression to castration-resistant prostate cancer.* Clin Cancer Res, 2010. **16**(17): p. 4319-24.
38. Jemal, A., et al., *Global cancer statistics.* CA Cancer J Clin, 2011. **61**(2): p. 69-90.
39. Jemal, A., et al., *Cancer statistics, 2009.* CA Cancer J Clin, 2009. **59**(4): p. 225-49.
40. Bellmunt, J. and W.K. Oh, *Castration-resistant prostate cancer: new science and therapeutic prospects.* Ther Adv Med Oncol, 2010. **2**(3): p. 189-207.
41. Kong, D., et al., *Androgen receptor splice variants contribute to prostate cancer aggressiveness through induction of EMT and expression of stem cell marker genes.* Prostate, 2015. **75**(2): p. 161-74.
42. Stanbrough, M., et al., *Increased expression of genes converting adrenal androgens to testosterone in androgen-independent prostate cancer.* Cancer Res, 2006. **66**(5): p. 2815-25.
43. Montgomery, R.B., et al., *Maintenance of intratumoral androgens in metastatic prostate cancer: a mechanism for castration-resistant tumor growth.* Cancer Res, 2008. **68**(11): p. 4447-54.
44. Hara, T., et al., *Novel mutations of androgen receptor: a possible mechanism of bicalutamide withdrawal syndrome.* Cancer Res, 2003. **63**(1): p. 149-53.
45. Schuurmans, A.L., et al., *Stimulatory effects of antiandrogens on LNCaP human prostate tumor cell growth, EGF-receptor level and acid phosphatase secretion.* J Steroid Biochem Mol Biol, 1990. **37**(6): p. 849-53.

46. Yoshida, T., et al., *Antiandrogen bicalutamide promotes tumor growth in a novel androgen-dependent prostate cancer xenograft model derived from a bicalutamide-treated patient.* Cancer Res, 2005. **65**(21): p. 9611-6.
47. Elo, J.P., et al., *Mutated human androgen receptor gene detected in a prostatic cancer patient is also activated by estradiol.* J Clin Endocrinol Metab, 1995. **80**(12): p. 3494-500.
48. Tan, J., et al., *Dehydroepiandrosterone activates mutant androgen receptors expressed in the androgen-dependent human prostate cancer xenograft CWR22 and LNCaP cells.* Mol Endocrinol, 1997. **11**(4): p. 450-9.
49. Bergerat, J.P. and J. Ceraline, *Pleiotropic functional properties of androgen receptor mutants in prostate cancer.* Hum Mutat, 2009. **30**(2): p. 145-57.
50. Dehm, S.M., et al., *Splicing of a novel androgen receptor exon generates a constitutively active androgen receptor that mediates prostate cancer therapy resistance.* Cancer Res, 2008. **68**(13): p. 5469-77.
51. Guo, Z., et al., *A novel androgen receptor splice variant is up-regulated during prostate cancer progression and promotes androgen depletion-resistant growth.* Cancer Res, 2009. **69**(6): p. 2305-13.
52. Hu, R., et al., *Ligand-independent androgen receptor variants derived from splicing of cryptic exons signify hormone-refractory prostate cancer.* Cancer Res, 2009. **69**(1): p. 16-22.
53. Xu, Y.M., et al., *Discovery of Potent 17beta-Hydroxywithanolides for Castration-Resistant Prostate Cancer by High-Throughput Screening of a Natural Products Library for Androgen-Induced Gene Expression Inhibitors.* J Med Chem, 2015. **58**(17): p. 6984-93.
54. Asangani, I.A., et al., *Therapeutic targeting of BET bromodomain proteins in castration-resistant prostate cancer.* Nature, 2014. **510**(7504): p. 278-82.
55. Sanford, M., *Enzalutamide: a review of its use in metastatic, castration-resistant prostate cancer.* Drugs, 2013. **73**(15): p. 1723-32.
56. Tannock, I.F., et al., *Docetaxel plus prednisone or mitoxantrone plus prednisone for advanced prostate cancer.* N Engl J Med, 2004. **351**(15): p. 1502-12.
57. Monn, M.F. and L. Cheng, *Emerging trends in the evaluation and management of small cell prostate cancer: a clinical and molecular perspective.* Expert Rev Anticancer Ther, 2016. **16**(10): p. 1029-37.
58. Hirano, D., et al., *Neuroendocrine differentiation in hormone refractory prostate cancer following androgen deprivation therapy.* Eur Urol, 2004. **45**(5): p. 586-92; discussion 592.
59. Aparicio, A.M., et al., *Platinum-based chemotherapy for variant castrate-resistant prostate cancer.* Clin Cancer Res, 2013. **19**(13): p. 3621-30.
60. Culine, S., et al., *Docetaxel and cisplatin in patients with metastatic androgen independent prostate cancer and circulating neuroendocrine markers.* J Urol, 2007. **178**(3 Pt 1): p. 844-8; discussion 848.
61. Flechon, A., et al., *Phase II study of carboplatin and etoposide in patients with anaplastic progressive metastatic castration-resistant prostate cancer (mCRPC) with or without neuroendocrine differentiation: results of the French Genito-Urinary Tumor Group (GETUG) P01 trial.* Ann Oncol, 2011. **22**(11): p. 2476-81.
62. Brenner, J.C., et al., *Mechanistic rationale for inhibition of poly(ADP-ribose) polymerase in ETS gene fusion-positive prostate cancer.* Cancer Cell, 2011. **19**(5): p. 664-78.
63. Wang, H.T., et al., *Neuroendocrine Prostate Cancer (NEPC) progressing from conventional prostatic adenocarcinoma: factors associated with time to development of NEPC and survival from NEPC diagnosis-a systematic review and pooled analysis.* J Clin Oncol, 2014. **32**(30): p. 3383-90.
64. Jemal, A., et al., *Cancer statistics, 2010.* CA Cancer J Clin, 2010. **60**(5): p. 277-300.

65. Beltran, H., et al., *Divergent clonal evolution of castration-resistant neuroendocrine prostate cancer.* Nat Med, 2016. **22**(3): p. 298-305.
66. Terry, S. and H. Beltran, *The many faces of neuroendocrine differentiation in prostate cancer progression.* Front Oncol, 2014. **4**: p. 60.
67. Williamson, S.R., et al., *ERG-TMPRSS2 rearrangement is shared by concurrent prostatic adenocarcinoma and prostatic small cell carcinoma and absent in small cell carcinoma of the urinary bladder: evidence supporting monoclonal origin.* Mod Pathol, 2011. **24**(8): p. 1120-7.
68. Otto, T., et al., *Stabilization of N-Myc is a critical function of Aurora A in human neuroblastoma.* Cancer Cell, 2009. **15**(1): p. 67-78.
69. Priemer, D.S., et al., *Neuroendocrine Tumors of the Prostate: Emerging Insights from Molecular Data and Updates to the 2016 World Health Organization Classification.* Endocr Pathol, 2016. **27**(2): p. 123-35.
70. Hsu, J.Y., et al., *Mitotic phosphorylation of histone H3 is governed by Ipl1/aurora kinase and Glc7/PP1 phosphatase in budding yeast and nematodes.* Cell, 2000. **102**(3): p. 279-91.
71. Slack, A., et al., *The p53 regulatory gene MDM2 is a direct transcriptional target of MYCN in neuroblastoma.* Proc Natl Acad Sci U S A, 2005. **102**(3): p. 731-6.
72. Beroukhim, R., et al., *The landscape of somatic copy-number alteration across human cancers.* Nature, 2010. **463**(7283): p. 899-905.
73. Kumari, A., W.P. Folk, and D. Sakamuro, *The Dual Roles of MYC in Genomic Instability and Cancer Chemoresistance.* Genes (Basel), 2017. **8**(6).
74. Chappell, J. and S. Dalton, *Roles for MYC in the establishment and maintenance of pluripotency.* Cold Spring Harb Perspect Med, 2013. **3**(12): p. a014381.
75. Kalkat, M., et al., *MYC Deregulation in Primary Human Cancers.* Genes (Basel), 2017. **8**(6).
76. Collins, S. and M. Groudine, *Amplification of endogenous myc-related DNA sequences in a human myeloid leukaemia cell line.* Nature, 1982. **298**(5875): p. 679-81.
77. Beltran, H., *The N-myc Oncogene: Maximizing its Targets, Regulation, and Therapeutic Potential.* Mol Cancer Res, 2014. **12**(6): p. 815-22.
78. Hatton, K.S., et al., *Expression and activity of L-Myc in normal mouse development.* Mol Cell Biol, 1996. **16**(4): p. 1794-804.
79. Shen, J., et al., *Prognostic significance of nuclear accumulation of c-myc and mdm2 proteins in synovial sarcoma of the extremities.* Oncology, 2000. **58**(3): p. 253-60.
80. Felsher, D.W. and J.M. Bishop, *Transient excess of MYC activity can elicit genomic instability and tumorigenesis.* Proc Natl Acad Sci U S A, 1999. **96**(7): p. 3940-4.
81. Kuzyk, A. and S. Mai, *c-MYC-induced genomic instability.* Cold Spring Harb Perspect Med, 2014. **4**(4): p. a014373.
82. Schwab, M., et al., *Amplified DNA with limited homology to myc cellular oncogene is shared by human neuroblastoma cell lines and a neuroblastoma tumour.* Nature, 1983. **305**(5931): p. 245-8.
83. Henriksson, M. and B. Luscher, *Proteins of the Myc network: essential regulators of cell growth and differentiation.* Adv Cancer Res, 1996. **68**: p. 109-82.
84. van Bokhoven, H., et al., *MYCN haploinsufficiency is associated with reduced brain size and intestinal atresias in Feingold syndrome.* Nat Genet, 2005. **37**(5): p. 465-7.
85. Sun, W., P.E. Sanderson, and W. Zheng, *Drug combination therapy increases successful drug repositioning.* Drug Discov Today, 2016. **21**(7): p. 1189-95.
86. Sertkaya, A., et al., *Key cost drivers of pharmaceutical clinical trials in the United States.* Clin Trials, 2016. **13**(2): p. 117-26.
87. Zheng, W., W. Sun, and A. Simeonov, *Drug repurposing screens and synergistic drug-combinations for infectious diseases.* Br J Pharmacol, 2018. **175**(2): p. 181-191.

88. Hoelder, S., P.A. Clarke, and P. Workman, *Discovery of small molecule cancer drugs: successes, challenges and opportunities.* Mol Oncol, 2012. **6**(2): p. 155-76.
89. McDermott, U., J.R. Downing, and M.R. Stratton, *Genomics and the continuum of cancer care.* N Engl J Med, 2011. **364**(4): p. 340-50.
90. Macarron, R., et al., *Impact of high-throughput screening in biomedical research.* Nat Rev Drug Discov, 2011. **10**(3): p. 188-95.
91. Administration, U.F.a.D., *FDA Approved Drug Products.* 2018.
92. Wong, L., *New results in biological sequence analysis, complex gene-disease association, qPCR calculation, and biological text mining.* J Bioinform Comput Biol, 2010. **8**(5): p. v-ii.
93. Malo, N., et al., *Statistical practice in high-throughput screening data analysis.* Nat Biotechnol, 2006. **24**(2): p. 167-75.
94. Brideau, C., et al., *Improved statistical methods for hit selection in high-throughput screening.* J Biomol Screen, 2003. **8**(6): p. 634-47.
95. Janssens, A., M. Boogaerts, and G. Verhoef, *Development of fludarabine formulations in the treatment of chronic lymphocytic leukemia.* Drug Des Devel Ther, 2009. **3**: p. 241-52.
96. Johnson, S., et al., *Multicentre prospective randomised trial of fludarabine versus cyclophosphamide, doxorubicin, and prednisone (CAP) for treatment of advanced-stage chronic lymphocytic leukaemia. The French Cooperative Group on CLL.* Lancet, 1996. **347**(9013): p. 1432-8.
97. Plunkett, W., et al., *Fludarabine: pharmacokinetics, mechanisms of action, and rationales for combination therapies.* Semin Oncol, 1993. **20**(5 Suppl 7): p. 2-12.
98. Huang, P., et al., *Inhibition of RNA transcription: a biochemical mechanism of action against chronic lymphocytic leukemia cells by fludarabine.* Leukemia, 2000. **14**(8): p. 1405-13.
99. Kemena, A., et al., *A sensitive fluorescence assay for quantitation of fludarabine and metabolites in biological fluids.* Clin Chim Acta, 1991. **200**(2-3): p. 95-106.
100. Foran, J.M., et al., *Pharmacokinetic study of single doses of oral fludarabine phosphate in patients with "low-grade" non-Hodgkin's lymphoma and B-cell chronic lymphocytic leukemia.* J Clin Oncol, 1999. **17**(5): p. 1574-9.
101. Oscier, D., et al., *The bioavailability of oral fludarabine phosphate is unaffected by food.* Hematol J, 2001. **2**(5): p. 316-21.
102. Lonardi, S., et al., *Oral anticancer drugs in the elderly: an overview.* Drugs Aging, 2007. **24**(5): p. 395-410.
103. Keating, M.J., et al., *Fludarabine: a new agent with major activity against chronic lymphocytic leukemia.* Blood, 1989. **74**(1): p. 19-25.
104. Smith, T.J., et al., *2006 update of recommendations for the use of white blood cell growth factors: an evidence-based clinical practice guideline.* J Clin Oncol, 2006. **24**(19): p. 3187-205.
105. Chun, H.G., et al., *Central nervous system toxicity of fludarabine phosphate.* Cancer Treat Rep, 1986. **70**(10): p. 1225-8.
106. Cheson, B.D., et al., *Tumor lysis syndrome: an uncommon complication of fludarabine therapy of chronic lymphocytic leukemia.* J Clin Oncol, 1998. **16**(7): p. 2313-20.
107. Bonin, M., et al., *F-ara-A pharmacokinetics during reduced-intensity conditioning therapy with fludarabine and busulfan.* Bone Marrow Transplant, 2007. **39**(4): p. 201-6.
108. Sun, L. and C.E. Lau, *Intravenous and oral clozapine pharmacokinetics, pharmacodynamics, and concentration-effect relations: acute tolerance.* Eur J Pharmacol, 2000. **398**(2): p. 225-38.
109. Lukenbill, J. and M. Kalaycio, *Fludarabine: a review of the clear benefits and potential harms.* Leuk Res, 2013. **37**(9): p. 986-94.

110. Yabe, H., et al., *Natural pregnancy and delivery after unrelated bone marrow transplantation using fludarabine-based regimen in a Fanconi anemia patient.* Int J Hematol, 2010. **91**(2): p. 350-1.
111. Rosenwald, A., et al., *Fludarabine treatment of patients with chronic lymphocytic leukemia induces a p53-dependent gene expression response.* Blood, 2004. **104**(5): p. 1428-34.
112. Wei, C.L., et al., *A global map of p53 transcription-factor binding sites in the human genome.* Cell, 2006. **124**(1): p. 207-19.